# The posterior parietal cortex of the rat: architectural delineation and thalamic differentiation

Grethe M. Olsen[1] and Menno P. Witter[1, 2]

[1]Kavli Institute for Systems Neuroscience, Centre for Neural Computation, Norwegian University of Science and Technology, The Faculty of Medicine, NTNU, Postboks 8905, 7491 Trondheim, Norway

[2]Correspondence to Menno P. Witter, Kavli Institute for Systems Neuroscience & Centre for Neural Computation, Medical-Technical Research Center
Postboks 8905
NO-7491Trondheim
NORWAY
Phone: +47 73598249
Email: menno.witter@ntnu.no

Abbreviated title: Architectural and thalamic definition of rat PPC
Number of text pages: 61
Number of figures: 21
Number of tables: 2
Number of words abstract: 242
Number of words introduction: 849
Number of words discussion: 4322
[1]

Keywords and RRIDs: anterograde tracer injections, retrograde tracer injections, immunohistochemistry, AB_477329, AB_94952, AB_258604, AB_10015300, AB_2336818, AB_2307337, AB_10000080, AB_2336881, AB_2532130, AB_142672, AB_142628, SCR_014199, SCR_014198, SCR_001775, SCR_003070

[1] This study was supported by the Kavli Foundation and Centre of Excellence (#145993), equipment (#181676), and research (#191929) grants from the Norwegian Research Council.

**Abstract**

In this study, we aim to refine the characterization of the rat parietal cortical domain in terms of cyto- and chemoarchitecture, as well as thalamic connectivity. We recognize three subdivisions of the posterior parietal cortex (PPC), which are architectonically distinct from the neighboring somatosensory and visual cortices. Furthermore, we show that the different parietal areas are differently connected with thalamic nuclei. The medial portion of PPC (mPPC) is primarily connected with the medial portion of the lateral posterior nucleus (LP), while the lateral portion (lPPC) connects with the posterior complex (Po). The more caudolateral part of PPC (PtP) also projects to Po but can be distinguished from lPPC based on architectonic criteria. The primary somatic and visual cortices, neighboring PPC, are preferentially connected with the primary ventral posterior and dorsolateral geniculate nuclei, respectively, and less with the associational Po and LP. Particularly the border between the secondary visual cortex and PPC has been a matter of controversy, but here we show that while PPC subareas are connected with Po and medial LP, the medial and lateral secondary visual cortices are connected with lateral LP and a portion of medial LP different from that connected with PPC. The resulting delineations and specifications of connectivity with thalamic nuclei together with upcoming studies of cortical connectivity will facilitate detailed studies on the role of the subdivisions of PPC in the rat as diverse, higher order associative cortical areas, comparable to those described in the primate.

## Introduction

The posterior parietal cortex (PPC) of the rat is a multimodal association area, proposed to play a role in directed attention and spatial navigation (Miller and Vogt, 1984; Kolb and Walkey, 1987). For instance, unilateral lesions of PPC produce contralateral neglect (King and Corwin, 1993), and animals with bilaterally lesioned PPC have difficulties navigating in a water maze (Kolb and Walkey, 1987; DiMattia and Kesner, 1988; Save and Moghaddam, 1996; Save and Poucet, 2000). Unfortunately, in these studies, large areas of the cortex were lesioned, meaning that visual and/or somatosensory areas have probably been affected in addition to PPC. Hence, hypothesized functions deduced from these lesions cannot with certainty be ascribed exclusively to PPC. Recording studies in freely behaving animals support a role in spatial information processing. Neurons in PPC have head-direction properties(Chen et al., 1994a; b), are sensitive to the animal's position in a labyrinth-like maze (Nitz, 2006; 2012), and are behaviorally tuned to specific modes of movement, irrespective of the animal's location or heading (Whitlock et al., 2012). In all these studies, recordings were generally done dorsomedially in PPC. A recent study found populations of neurons across medial and lateral subdivisions of dorsal PPC that coded for self-motion, head direction, and the direction to a goal relative to the animal's head (Wilber et al., 2014). None of the above mentioned studies investigated the function of the caudolateral portion of PPC.

Probing the functional relevance of PPC has been complicated by the fact that the physical location and delineation of PPC in the rat cortex is still debated (for a review, see Whitlock et al., 2008). Delineations of cortical areas can be based on various methods, such as architectonics, patterns of connectivity, or as seen above, electrophysiological properties of cells in the area. In the rat brain, a parietal area 7 was first identified based on cyto- and

myeloarchitectonics (Krieg, 1946b) and, similar to studies in other species, it was found to be located between the dorsomedial part of the primary parietal (somatosensory) area and the occipital region. However, in two later studies, also using cytoarchitectonic criteria, it was suggested that the region corresponding to Krieg's area 7 consisted of a posterior parietal portion with a secondary visual portion immediately caudal to it, although the two studies disagree on the lateral extent of PPC (Miller and Vogt, 1984; Burwell and Amaral, 1998). In another study, the distribution of receptor densities was used to characterize the region corresponding to Krieg's area 7 (Palomero-Gallagher and Zilles, 2004). Deviating from the earlier studies, the latter authors considered the dorsomedial portion of the region to be visual cortex, while the more caudolateral portion was recognized as parietal. In sharp contrast, two recent studies denominated the entire dorsomedial region as parietal cortex, since neurons along the rostral-caudal axis appeared to have similar functional and connectional characteristics (Wilber et al., 2014; 2015).

Thus, architectonic and functional features alone are not sufficient to consistently delineate parietal divisions. Early studies postulated that an observed topography in thalamic projections to the cortex was related to functional differences between cortical areas (Lashley, 1941). It is now known that cortical areas also project back to specific nuclei of the thalamus, although it is debated whether these projections reciprocate the thalamocortical projections in a strict manner (Deschenes et al., 1998). In a study of thalamic connectional patterns of parietal cortex in the rat using fluorescent retrograde tracers (Chandler et al., 1992), PPC was defined as having input from three associational thalamic nuclei, the laterodorsal (LD), lateral posterior (LP) and the posterior nuclei (Po). PPC did not receive input from the primary somatosensory ventral posterior (VP; VB in the original paper) nor primary visual dorsolateral geniculate nuclei (DLG). A later study found that at least parts of PPC

reciprocated the input from the three associational thalamic nuclei mentioned above (Kamishina et al., 2009). Thus, the organization of the reciprocal thalamic-cortical connections could provide additional means to differentiate between parietal areas, yet the correlative information on how thalamic and architectonic criteria are related is currently insufficient to divide PPC in the rat.

The lack of a clear and disambiguous definition of PPC hampers a detailed analysis in at least three ways. First, it is difficult to determine whether connectional differences and topographies exist within PPC. Some tracing studies of PPC observed variations in the thalamic connectivity of the medial versus lateral portions of PPC, but did not explore this in detail (Reep et al., 1994; Kamishina et al., 2009). A recent study found significant differences in connectivity between medial and lateral portions of dorsal PPC, but did not investigate the caudolateral subregion (Wilber et al., 2015). Second, a coherent interpretation of functional data also depends on a commonly accepted delineation of PPC. Finally, it is still unclear whether the rat PPC may comprise functionally different divisions comparable to those for example described in primates (Rawley and Constantinidis, 2009; Wilber et al., 2014). In this study, we used a combination of cyto- and chemoarchitectural criteria, complemented with patterns of thalamic connectivity to delineate areas in the dorsal caudal cortex of the rat brain.

## Materials and methods

We used 52 adult Sprague Dawley rats (Charles River, Sulzfeld/Kisslegg, Germany), two for architectural studies and 50 for tracer injections. The rats were group-housed with food and water available ad libitum. After surgery, the animals were individually housed until

euthanasia. All experimental procedures followed locally approved protocols that adhere to national and EU regulations.

Histology for coronal delineations

One adult male Sprague Dawley rat (540 g) was anesthetized with an intraperitoneal injection of Equithesin (provided by the local pharmacy; main effective ingredients are chloral hydrate, magnesium sulphate heptahydrate, and pentobarbital) and transcardially perfused using a peristaltic pump (World precision instruments, Hertfortshire, England), first with a Ringer's solution (0.85% NaCl, 0.025% KCl, 0.02% $NaHCO_3$, 37°C, pH 6.9) and then with a freshly depolymerized 4% paraformaldehyde solution (pH 7.4; Merck Chemicals, Darmstadt, Germany) in 0.125 M phosphate buffer containing 0.25% glutaraldehyde (Merck Chemicals). The brain was extracted and left in a 4% paraformaldehyde solution overnight before being cryoprotected in a DMSO/glycerol solution (2% Dimethyl Sulfoxide and 20% glycerol in 0.125 M phosphate buffer; DMSO and glycerol from VWR, Radnor, PA). The two hemispheres of the brain were separated along the midline, and on a freezing microtome (Thermo Scientific, Pittsburgh, PA), 30 µm sections were prepared in six equally spaced series for each hemisphere. One hemisphere was cut in the coronal plane while the other was cut sagitally. For each hemisphere, one series of sections was mounted in sequence on Superfrost plus-slides (Thermo Scientific) and stained with cresyl violet (Sigma-Aldrich, St. Louis, MO), one series was stained for parvalbumin and one for the type 2 muscarinic acetylcholine receptor (M2AChR) using a standard immunohistochemical protocol.

Primary antibody against parvalbumin was obtained from Sigma-Aldrich (monoclonal mouse anti-parvalbumin, catalog number P3088, RRID: AB_477329, see also Table 1). According to

the vendor, the antibody is raised against purified frog muscle parvalbumin and the isotype is determined by a double diffusion immunoassay. It reacts with 12 kDa parvalbumin originating in a range of species including rats, while it does not react with other calcium-binding proteins of the same family. Previous studies have proved the specificity of the antibody, for instance it recognized the calcium binding sites of parvalbumin in a Western blot analysis (Cerkevich et al., 2013) and the isotype has been confirmed using standard kits for this procedure (Gray et al., 2014). No specific staining was observed after preadsorption of the antibody with recombinant rat parvalbumin-α, staining sections from a parvalbumin-β gel, staining tissue from parvalbumin knockout-mice, or omitting the secondary antibody in a standard immunohistochemical procedure (Hackney et al., 2005; Ding and Weinberg, 2007; Burette et al., 2009).

Primary antibody against M2AChR was purchased from Merck Millipore (Billerica, MA; affinity purified monoclonal rat anti-M2AChR, catalog number MAB367, RRID: AB_94952, see also Table 1). The antibody is raised against a recombinant protein fused to Glutathione S-transferase. The recombinant protein is derived from the putative third inner cytoplasmic loop of the human M2 receptor (M2i3, amino acids 225-359) (Levey et al., 1995), the i3 loop is specific for each receptor subtype (Levey et al., 1990; Levey et al., 1991). The labeling pattern after immunohistochemistry with the monoclonal antibody has been found identical to when a polyclonal antibody is used (Levey et al., 1995), the specificity of which has been described in immunoblotting and immunoprecipitation studies (Levey et al., 1990; Levey et al., 1991). Only background staining has been observed after staining of tissue from M2 or M2/M4 receptor subtype specific knockout mice (Duttaroy et al., 2002). The antibody has previously been used to help delineation of areas in the mouse caudal cortex (Wang et al., 2011).

Free floating sections were first rinsed with 0.125 M phosphate buffer and then permeabilised with Tris-buffered saline (0.606% Tris(hydroxymethyl)aminomethane, 0.896% NaCl, pH 8.0; VWR) containing 0.5% Triton X-100 (TBS-TX) before being incubated with primary antibody (1:1000 mouse anti-parvalbumin or 1:750 rat anti-M2AChR;) in TBS-TX for 24 hours at room temperature. Sections were rinsed with TBS-TX and incubated with biotinylated secondary antibody (1:200 goat anti-mouse, Sigma-Aldrich, catalog number B7151, RRID: AB_258604; or 1:300 rabbit anti-rat, Vector Laboratories, Burlingame, CA, catalog number BA-4001, RRID: AB_10015300) in TBS-TX for 90 minutes at room temperature. Sections were then washed with TBS-TX and incubated with an avidin-biotin complex (Vector Laboratories, RRID: AB_2336818) in TBS-TX for 90 minutes at room temperature, before labeling was visualized using a 0.067% 3,3'-Diaminobenzidine tetrahydrochloride (DAB, Sigma-Aldrich, catalog number D5905) solution in Tris buffer (0.606% Tris(hydroxymethyl)aminomethane, VWR; pH adjusted to 7.6 using HCl) containing 0.08% $H_2O_2$ (Sigma-Aldrich). The sections were finally rinsed in Tris buffer and mounted on uncoated Menzel-glass microscope slides (Thermo Scientific) from a Tris-gelatin solution (0.2% gelatin in Tris buffer, pH 7.6), air-dried, defatted in xylene, and coverslipped using Entellan (Merck Chemicals) as mounting medium.

The sections were digitalized using a Mirax-midi brightfield scanner (objective 20X, NA 0.8; Carl Zeiss Microscopy, Jena, Germany). For coronal sections, pictures were captured of all sections that were in the range of 0.6-5.4 mm caudal to bregma. Brightness and contrast was adjusted using Adobe Photoshop CS6 (Adobe Systems Incorporated, San Jose, CA; http://www.adobe.com/no/products/cs6.html; RRID: SCR_014199) and the images were

imported to Adobe Illustrator CS6 (Adobe Systems Incorporated; http://www.adobe.com/no/products/cs6.html; RRID: SCR_014198). Images of corresponding sections with the three stains were overlayed and borders of cortical areas were drawn. Having defined cortical areas in overlays, for five different coronal levels, high resolution images of sections stained for Nissl, M2AChR and parvalbumin were aligned next to each other and borders were drawn on each image using Adobe Illustrator.

Flattened brain

One adult male Sprague Dawley rat (470 g) was given an intraperitoneal overdose of Equithesin and perfused transcardially first with a Ringer solution (37°C, pH 6.9) and then with a freshly depolymerized 2% paraformaldehyde solution in 0.125 M phosphate buffer (pH 7.4). The brain was extracted and put in 0.125 M phosphate buffer overnight. The following day, the brain was cut in half along the midline. For both hemispheres, another cut was made starting in front of the hippocampus dorsally and ending up in front of the entorhinal/amygdaloid transition ventrally, keeping only the caudal part of the brain. The cerebral cortex was dissected out and flattened between two regular microscope slides covered with parafilm (Pechiney plastic packaging, Chicago, IL). Sponges were put next to the tissue to avoid the slides being pressed together too hard and thus squeezing the tissue. The two microscope slides were taped together and the whole construct was immersed in a 4% paraformaldehyde solution overnight and then cryoprotected in DMSO/glycerol solution. After cryoprotection, the flattened cortex was released from the slides and cut tangentially on a freezing microtome, starting at the pial surface. 30 µm thick sections were collected in four equally spaced series. For each hemisphere, one series was mounted on Superfrost plus-slides and stained for Nissl using cresyl violet, while another series of free floating sections was

stained for M2AChR using a DAB reaction. The immunohistochemical staining procedure was similar to the procedure described above, except the incubation time for the primary antibody was slightly shorter (17 hours). Similar to the case described above, the stained sections from this brain were mounted on microscope slides and digitalized using a Mirax-midi brightfield scanner. High resolution pictures of two M2AChR stained sections were overlayed in Adobe Photoshop using the clearly differentiable barrels in layer 4 of the primary somatosensory cortex as fiducial marks. A maximum projection of both pictures was imported into Adobe Illustrator, where it was compared to pictures of Nissl stained sections and outlines of cortical areas were drawn.

Tracer injections

The brains of 50 young adult female Sprague Dawley rats (180-230 g at the time of surgery) were injected with retrograde and anterograde tracers. The retrograde tracers used were Fast Blue (EMS Chemie, Domat/Ems, Switzerland, catalog number 9000002; 1% in 0.125 M phosphate buffer), Fluorogold (Fluorochrome, Denver, CO; 2.5% in $H_2O$), and Diamidino Yellow (EMS Chemie, catalog number 9000006; 2% in $H_2O$); for anterograde tracing, *Phaseolus vulgaris* Leucoagglutinin (PHA-L, Vector Laboratories, catalog number L-1110; 2.5% in 0.01 M phosphate buffer) and 10 kDa biotinylated dextran amine (BDA, Invitrogen, Molecular Probes, Eugene, OR, catalog number D1956, RRID: AB_2307337; 5% solution in 0.125 M phosphate buffer) were used. The rats were anesthetized with Isoflurane and injected i.p. with atropine (Nycomed, Zürich, Switzerland, 0.04 mg/kg) and rimadyl (Pfizer, New York, NY, 5 mg/kg) before being placed in a stereotaxic frame (Kopf Instruments, Tujunga, CA) on top of a heating pad maintaining a constant temperature of 37°C. The head was shaved dorsally and an incision in the skin was made along the midline of the head.

Stereotaxic coordinates were determined using bregma and the midsagital sinus as rostral-caudal and medial-lateral reference points, respectively, using a stereotaxic atlas as a guide (Paxinos and Watson, 2007). In several animals, multiple tracer injections were made (see below for details). A burr hole through the skull was made at the intended injection coordinate(s) and the dura was perforated using a micro knife (Fine Science Tools, Heidelberg, Germany). Retrograde tracers were pressure-injected into the brain through 1 µl Hamilton syringes. Iontophoretic injections of anterograde tracers were performed using glass micropipettes with an outer tip diameter of 15-25 µm (alternating currents, 6 seconds on/6 seconds off, 6 µA for BDA and 7 µA for PHA-L). During the surgery, the rat was given saline subcutaneously to avoid dehydration. Upon completion of injections, the wound was cleaned and sutured, and the animal was allowed to recover in a heat chamber before being returned to its home cage.

After a survival period of 1-2 weeks, animals were given an overdose of Equithesin and perfused transcardially with a Ringer solution (37°C, pH 6.9) followed by freshly depolymerized 4% paraformaldehyde (pH 7.4) in 0.125 M phosphate buffer. The brains were extracted and postfixed in the perfusion fixative overnight. After being cryoprotected in a DMSO/glycerol solution at least overnight, six equally spaced series of 50 µm coronal sections were prepared on a freezing microtome. One series was mounted on Superfrost plus-slides and stained with cresyl violet for cytoarchitectural orientation. For brains containing fluorescent retrograde tracer(s), one series was mounted on uncoated microscope slides for analysis without any further processing. For brains containing anterograde tracer(s), one series was stained for BDA and/or PHA-L. While visualization of BDA requires a histochemical reaction with streptavidin or an avidin/biotin complex, visualization of PHA-L necessitates an immunohistochemical procedure. Primary antibody against PHA-L was obtained from Vector

laboratories (affinity purified polyclonal goat anti-PHA-L, catalog number AS-2224, RRID: AB_10000080; see also Table 1). According to the vendor, the antibody is raised in goats against pure lectins, and is affinity purified by chromatography on lectin-agarose columns. According to the datasheet, the antibody reacts strongly with *Phaseolus vulgaris* erythroagglutinin and leucoagglutinin (PHA-E + L). In a previous study employing the same antibody, no labeling was observed after immunohistochemical processing of tissue that had not been injected with PHA-L, whereas reaction product in PHA-L injected tissue was confined to the injection site and anterogradely labeled axons (Zahm et al., 2013).

In our experiment, free floating sections were first rinsed in 0.125 M phosphate buffer and permeabilised with TBS-TX (pH 8.0) before being incubated with goat anti-PHA-L (1:1000) in TBS-TX at room temperature overnight. The following day, the sections were rinsed with TBS-TX before being incubated in TBS-TX containing fluorophore-tagged streptavidin (1:200, Invitrogen, Molecular Probes, AlexaFluor® 488, catalog number S11223, RRID: AB_2336881 or AlexaFluor® 546, catalog number S11225, RRID: AB_2532130) and/or donkey anti-goat (1:400, Invitrogen, Molecular Probes, AlexaFluor® 488, catalog number A11055, RRID: AB_142672 or AlexaFluor® 546, catalog number A11056, RRID: AB_142628) for 2 hours at room temperature to visualize BDA and PHA-L, respectively. For some brains, additional series were single stained for BDA or PHA-L using DAB as the final chromogen. Some of the series of sections in which we visualized anterograde tracers were subsequently counterstained with cresyl violet. Stained sections were mounted on regular microscope slides, air dried, defatted in xylene and coverslipped using Entellan as mounting medium.

The positions of individual injection sites were assessed based on cytoarchitectonic criteria and mapped onto a 3D representation of the rat brain using Neurolucida (MicroBrightField, Colchester, VT, http://www.mbfbioscience.com/neurolucida; RRID: SCR_001775). Since our analysis to a large extent corroborated the PPC subdivisions as indicated in the Rat Brain Atlas (Paxinos and Watson, 2007), we used that dataset to prepare the final illustrations of the injection sites. The core of the injection site was drawn in the section taken from the atlas at the corresponding bregma level, and then copied into one section more rostral and one section more caudal in order to create a 3D representation of the injection site. Finally, borders of cortical areas according to the atlas were entered in the Neurolucida file. An image of the surface of the 3D representation was imported to Adobe Illustrator and overlaid with a picture of an intact rat brain, and the borders of cortical areas were indicated onto the cortical surface. The position and extent of the injection sites were mapped as well and each injection site was given the proper denomination according to the animal number and tracer injected.

For cases injected with retrograde tracers, mounted sections were investigated with the use of a Zeiss Axio Imager M2 examiner (Carl Zeiss Microscopy), using an appropriate excitation wavelength. The outline of selected sections and the distribution of retrogradely labeled neurons were mapped using Neurolucida. With the use of Adobe Illustrator, exported Neurolucida images of the labeling pattern were later overlaid on pictures of Nissl stained sections at the corresponding level from the same brain for delineation of thalamic nuclei. For illustration purposes, images of sections at the following bregma-levels were chosen for each case (values may vary between cases): B-2.0, -2.5, -3.1, -3.5, -4.2, and -4.8 mm.

Mounted sections from cases with injections of anterograde tracers were scanned using a Mirax-midi fluorescent scanner (objective 20X, NA 0.8; Carl Zeiss Microscopy). Pictures were exported as high resolution bitmap files and converted to pseudo-darkfield images with the use of Adobe Photoshop. Brightness and contrast were adjusted. For two cases where two tracer injections were illustrated, the pseudo-colored signal was maintained for both channels. Using ImageJ (http://rsb.info.nih.gov/ij/index.html; RRID: SCR_003070), the two channels were split and brightness and contrast was adjusted for each channel separately. Images of labeling were imported into Adobe Illustrator, and overlaid on images of Nissl stained sections at the corresponding level from the same brain. Borders of thalamic nuclei were drawn based on images of the Nissl-stained sections and these borders were merged with the labeling images. Finally, the thalamic nuclei were denominated according to the Rat Brain Atlas (Paxinos and Watson, 2007). Abbreviations used for thalamic nuclei are listed in Table 2.

## Results

### Topography and nomenclature

The posterior parietal cortex (PPC) is wedged between the somatosensory and visual cortices (Fig. 1). It is a thin strip of cortex that comprises a dorsal and a ventral limb (Burwell and Amaral, 1998). In line with the majority of studies published about the rat PPC, we subdivided the dorsal limb in a medial and lateral division (mPPC and lPPC). The ventral limb has been named posterior part of parietal cortex (PtP; Paxinos and Watson, 2007). Although the latter authors subdivided PtP into dorsal, rostral, and caudal portions, we have grouped these subdivisions into one region. The PPC is bordered medially by the secondary motor area (M2, not shown) in rostral sections, and the medial secondary visual cortex (V2M) in more caudal sections. Medially, M2 and V2M are bordered by the retrosplenial cortex

(RSC, not shown), which forms the medial wall of the caudal half of the hemisphere. In our material, we did not find RSC to border PPC at any rostrocaudal level. Rostral to PPC, one finds the primary motor cortex (M1, not shown) and the primary somatosensory cortex (S1), extending also slightly lateral to PPC. S1 is replaced by auditory cortex (AuD, not shown) at more caudal levels. Caudally, PPC is bordered by the visual cortex. Primary visual cortex (V1) is bordered by secondary visual cortex medially (V2M) and laterally (V2L).

Architectural features of cortical areas

The use of the three different stains, Nissl, the type 2 muscarinic acetylcholine receptor (M2AChR) and parvalbumin, revealed specific staining patterns for and borders between the three PPC divisions, as well as with their respective neighbors. Moreover, the borders used were corroborated with the connectional data described below.

*Nissl stained sections*

In Nissl-stained sections, PPC appeared homogenous and a clear lamination was lacking (Fig. 2, left column), although lPPC showed a somewhat clearer lamination than mPPC. The cell density in layer 5 of mPPC was higher than that in layer 5 of lPPC. Laterally, in PtP, cells were less densely packed than in the other two portions of PPC. Layer 5 of PtP contained fewer pyramidal cells than the surrounding cortical areas, and neurons in layer 3/4 were small and weakly stained. Rostral to PPC, S1 was most easily recognized by its clear lamination and characteristic, dense granular layer 4. However, this feature was less prominent in the caudodorsal portion of S1 close to PPC, complicating an exact differentiation between the two areas. Layers 2 and 3 of S1 were wide. In layer 5, there was a cell-sparse zone superficially

and deeply, not seen in PPC. Medial and caudal to mPPC, V2M also appeared homogenous as well as poorly laminated, making the distinction from mPPC difficult. However, the neuronal packing in layer 5 of V2M appeared slightly denser than layer 5 of mPPC, and layers 2/3 were narrower in V2M than in mPPC. The more lateral V1 had a prominent granular layer 4 and a clear lamination. As in S1, layer 5 of V1 had a cell-sparse zone superficially and deeply. V2L, similar to V2M, appeared homogenous and not well laminated. The border between layers 4 and 5 was diffuse. Rostral to V2M, in M2, neurons in layer 3 were weakly stained. Although lamination in M2 was weakly developed, similar to mPPC, the two areas were different in that M2 layer 5 appeared more homogenously and densely packed, and superficial layers were narrower compared to mPPC. In M1, rostral to mPPC, layers 2 and 3 were wider than in M2, having the same width as the laterally adjacent S1. Layer 5 of M1 was less densely packed compared to M2 and contained considerably larger pyramidal cells. For RSC, we will only describe the cytoarchitectonic features of the dorsal dysgranular area 30. In this area, layers 2 and 3 were condensed but clearly differentiable from each other. Scattered granule cells could be found in layer 4, while layer 5 was sparsely packed with big pyramidal cells. These features provided clear border markers with the adjacent M2 in rostral sections and V2M in caudal sections.

*M2AChR stain*

Overall, staining for the type 2 muscarinic acetylcholine receptor M2AChR gave labeling that was quite similar across areas, although subtle variations in the staining could be seen (Fig. 2, middle column). Typically, cell nuclei did not stain for this receptor. In all areas, layer 4 and deep layer 5/superficial layer 6 contained the heaviest labeling whereas superficial layer 5 was only weakly labeled in most areas. The most prominent feature in mPPC was the relatively

dense and homogenous dendritic labeling in superficial layers. This kind of labeling was present only in patches of lPPC, where in addition the labeling in deep layers was less dense than in mPPC. Labeling in PtP was overall weaker than in mPPC or lPPC. Compared to PPC as a whole, S1 as well as V1 had a sharper differentiation between layers 4 and 5. Very prominent in V1 was dense dendritic labeling in superficial layers. Areas V2M and V2L showed homogenous staining across layers, similar to PPC, although the weaker dendritic labeling in these visual areas differentiated them from PPC. In M2, superficial layers were weakly stained and deep layers could barely be separated from each other. Particularly, the first feature demarcates the border with mPPC, the latter having dense dendritic labeling in superficial layers. In RSC, we observed a characteristic dense stripe of labeling in layer 3/4, while the other layers were homogenously and weakly stained. This staining pattern reliably differentiated RSC from its neighboring areas M2 and V2M.

*Parvalbumin stain*

The PPC contained little parvalbumin labeling compared to most of its neighboring areas (Fig. 2, right column). In mPPC, a few labeled cells were found, without showing a clear laminar preference. Neuropil labeling was virtually absent in mPPC. In lPPC, more cells were parvalbumin positive than in mPPC, and clearly labeled neuropil was seen, especially in the deep portion of layer 5 with weaker labeling in layers 2-4. PtP also contained weak labeling, with scattered labeled cells in all layers. The rostral border of mPPC with M1 was not striking, although M1 contained some labeled cells and neuropil in layers 4 and deep 5, not seen in mPPC. The medial border between mPPC and M2 was difficult to ascertain with the use of parvalbumin staining, since M2, like mPPC, was practically devoid of labeling. This feature demarcated M2 from M1. Area V2M differed from both mPPC and M2 in that it

showed neuropil labeling in deep layer 5, but not so much in other layers. This feature was true for all parts of V2, in which labeled cells were also scattered throughout the depths of the cortex. V1 as well as S1 contained distinctly labeled neuropil in layer 4, in addition to deep layer 5. Labeled cells were seen in all cell layers in both areas. Along the entire rostrocaudal extent of the medial caudal cortex, RSC was strongly labeled in layers 2/3 and 5; the labeling was strongest in the ventral portion and gradually got weaker close to the border with M2 and V2M.

Flat map

A tangential section through layer 4 of the cortex taken from a flattened hemisphere stained for M2AChR provided an additional way to appreciate the topology of the caudal hemisphere (Fig. 3), particularly when compared to figures 1 and 2. Borders between cortical areas were drawn based on staining patterns. Similar to findings in the mouse brain (Wang et al., 2011), we observed dense M2AChR staining in the rat brain in layer 4 of the primary sensory areas S1 (somatosensory), V1 (visual) and Au1 (auditory), as well as in the retrosplenial cortex. Within S1, the individual barrels of the barrel cortex were clearly marked. Also prominent was area V2M, which was virtually devoid of M2AChR labeling in layer 4. Other areas had varying degrees of labeling and borders between them are practically impossible to discern unless the labeling pattern is seen in combination with other stains and/or electrophysiological methods (as in Wang et al., 2011). In adjacent Nissl stained flattened sections, some differences in staining patterns could be seen between areas. For instance, in the primary visual cortex (Fig. 3, inset 1), cells in layer 4 were moderately stained, and a tendency for the cells to organize in semi-circular clusters was discernible. In the barrel cortex (Fig. 3, inset 3), individual barrels in layer 4 were visible. In contrast, in the posterior parietal cortex (Fig. 3,

inset 2), the cells were weakly stained and not organized in clusters. This can be related to the pattern seen in coronal sections (see left column in Fig. 2) where it is clear that the primary sensory areas S1 and V1 are distinctly laminated with a dense packing of cells in layer 4, while the higher order association area PPC appears more homogenous.

Injections of retrograde tracers

Fig. 4 shows the location of the cores of injection sites for all retrograde (Fig. 4A) and anterograde (Fig. 4B) tracers that have been analyzed in this study. We analyzed 32 injections of retrograde tracers (Fig. 4A) in the parietal and occipital domains of the cortex, of which 7 were in PPC (4 in mPPC, 3 in lPPC), 13 involved the primary somatosensory cortex (8 in dorsomedial and 5 in lateral S1) and 12 were in the visual cortex (8 in V1, 4 in V2M). None of the illustrated injections encroached on the white matter.

*Injections in PPC*

*mPPC.* Four injections of retrograde tracers were located throughout the rostrocaudal extent of mPPC (Fig. 4A). A representative injection of Fast Blue rostrally in mPPC (13079FB, Figs. 4A, 5), possibly extending into the somatosensory cortex, resulted in a high density of retrogradely labeled cells in the lateral posterior nucleus (LP, Fig. 5D) on the border between the medial and lateral portion. Most of the labeled cells were located ventrally in the nucleus. In more caudal sections, labeled cells were mainly focused in the ventral rostromedial portion of LP (LPmr, Fig. 5E). Moderate labeling was seen rostrodorsally in the ventral anterior/ventrolateral complex (VA/VL, Fig. 5A, B). A patch of labeled cells was found rostrally in the dorsolateral part of the anteromedial nucleus (AM, Fig. 5A), while a lower

number of labeled cells occurred in the posterior complex (Po) and the lateral portion of the ventral posterior complex (VPl, Fig. 5C-E). A few labeled cells were seen in nucleus reuniens (Re), the rhomboid nucleus (Rh), the centrolateral nucleus (CL), the mediodorsal nucleus (MD), the lateral dorsal nucleus (LD), the parafascicular nucleus (PF) and the periaqueductal gray (PAG).

Injecting Fast Blue more caudally in mPPC (13080FB, Figs. 4A, 6), likely involving a small part of the medial secondary visual cortex, led to a distribution of retrogradely labeled cells in the thalamus, similar to that following the rostral injection. In particular, LPmr contained a high number of labeled cells, but their location was more widespread within the nucleus than in the previous case, involving almost the complete mediolateral and dorsoventral extent of LPmr (Fig. 6D, E). In addition, relatively more labeled cells were located in the lateral LP (LPl, Fig. 6D, E) as well as LD (Fig. 6B, C) compared to the previous case. In contrast, no labeled cells were located in either portions of VP in the caudal case (Fig. 6B-F). The presence of labeled cells in VP for the rostral case and more widely distributed labeled cells in LP and LD in the caudal case can be explained by the involvement of S1 and V2M, respectively (compare with Figs. 8 and 10 for labeling patterns after injections of tracers in these areas). This leaves LPmr as the main thalamic input to mPPC.

*lPPC.* Three injections of retrograde tracers were centered caudally in lPPC (Fig. 4A). A big, representative injection of Fast Blue had its core in caudal lPPC (16309FB, Figs. 4A, 7) but extended both rostrally and caudally, likely involving somatosensory and visual cortices. This injection gave rise to a dense pattern of labeled cells throughout most of the rostrocaudal extent of Po (Fig. 7B-F) and LP (Fig. 7C, D). A small dense cluster of cells was also seen in

VP (Fig. 7A-E). In addition, labeled cells were observed in AM, Rh, Re, the ventromedial nucleus (VM), VA/VL, LD, CL, MD, the dorsolateral geniculate nucleus (DLG), PF, and PAG (Fig. 7). In two other cases with injections of tracer in lPPC (Fig. 4A, not shown), the densest clusters of labeled cells were found in Po while only a small patch of labeled cells was seen in LPmr. Considering the three cases together, Po appears to provide the main thalamic input to lPPC.

*Injections in the primary somatosensory cortex*

All injections in primary somatosenosory cortex (N=13; Fig. 4A) resulted in comparable levels and distributions of retrogradely labeled cells in the thalamus with preferential labeling in VA/VL, VP, and Po. A representative injection of Fast Blue caudally in the medial portion of the primary somatosensory cortex (15942FB, Figs. 4A, 8) resulted in dense clusters of retrogradely labeled cells in VA/VL, VPl and Po (Fig. 8). Some labeled cells were also seen in AM, Rh, Re, VM, LP, mainly LPmr, MD and PAG. Injections of retrograde tracers into the laterally situated barrel cortex (Fig. 4A, labeling patterns are not illustrated) resulted in labeled cells in the medial part of VP (VPm) rather than the lateral portion. Labeled cells were located more ventrolateral in Po in these cases than after injections of tracers in medial somatosensory cortex.

*Injections in the visual cortex*

*V1.* All injections into the primary visual cortex (N=8; Fig. 4A) yielded comparable patterns of labeled neurons in the thalamus, in particular the DLG contained a dense cluster of strongly labeled cells in all cases. In a representative case with an injection of Fast Blue in V1

(13162FB, Figs. 4A, 9) a dense cluster of labeled cells was clearly present in DLG (Fig. 9D-F). Another, small cluster of labeled cells was seen ventrally in LPmr at the most caudal level of this nucleus (Fig. 9E). This labeling was consistent between all retrograde tracer injections in V1. Lower numbers of labeled cells were also observed in other parts of LPmr, as well as LPl, LD, Po, AM, VM, Re, Rh, CM, CL, MD and PF.

*V2.* In contrast to the V1 cases, injections of tracers into the medial portion of secondary visual cortex (N=4; Fig. 4A) did not result in high numbers of retrogradely labeled neurons in DLG. A representative injection of Fast Blue (12948FB, Figs. 4A, 10) gave rise to a dense cluster of labeled cells in both medial and lateral portions of LP (Fig. 10C-E) as well as in Po (Fig. 10C-F). Within LPmr, the majority of labeled cells was found at a mid-dorsoventral level although some were observed also ventromedially. Po labeling was less dense in other cases, but still present. A small cluster of labeled cells was seen in DLG (Fig. 10D, E). Labeled cells were also seen in LD, AM, AV, Re, Rh, CL and PF. Another case with an injection in V2M (12947FG, Fig. 4A) also had a few labeled cells in DLG, whereas two other cases did not (16276FB and 13162DY, Fig. 4A). This could be explained by the more lateral location of the former injections, likely involving V1. Thus, V2M receives its main thalamic input from medial and lateral subdivisions of the LP nucleus.

Injections of anterograde tracers

We analyzed a total of 51 injections (Fig. 4B) of anterograde tracers in the parietal and occipital domains of the cortex, of which 22 were in PPC (7 in mPPC, 9 in lPPC, 6 in PtP), 13 involved the somatosensory cortex (4 in dorsomedial and 9 in lateral S1) and 16 were in the visual cortex (8 in V1, 7 in V2M, 1 in V2L). As can be seen from figure 4B, injections of

anterograde tracers tended to spread over a smaller area than injections of retrograde tracers (Fig. 4A), and labeling patterns from injections in different areas showed less overlap. Figure 11 shows an overview of the injection sites described below as seen in coronal sections. Injections did not encroach on the cortical white matter. In all cases, labeled axons were seen to leave the injection sites and join the underlying cortical white matter, from where they entered the internal capsule and reached the thalamus through the reticular nucleus where they gave off collaterals.

*Injections in PPC*

*mPPC.* Injections in mPPC (N=7; Fig. 4B) were distributed throughout the rostral-caudal axis of this area, most of them were located laterally close to the border with lPPC (see Fig. 4B). A representative case for the rostral part of mPPC had an injection site of PHA-L that extended slightly into the rostrally adjacent somatosensory cortex (13234P, Figs. 4B, 11, 12). The injection involved all layers of the cortex, with a core in layers 4 and 5 (Fig. 11). Moderate labeling was seen caudally in the lateral half of the medial lateral dorsal nucleus (LDm, Fig. 12B). The labeling continued and grew stronger caudally, extending into the lateral half of LPmr where the labeling was strongest (Fig. 12C, D). The patch of labeling in LPmr was ventrally located, and continuous with labeling in Po (Fig. 12C, D). There was also a second patch of labeled fibers more medially in LPmr (Fig. 12D). Even more caudally, LP labeling disappeared while some remained in Po (Fig. 12E, F). Within Po, labeling at rostral levels was located laterally and dorsally, whereas at more caudal levels the labeling took a more medial position. In addition, labeled fibers were seen dorsally in the reticular nucleus (Rt, Fig. 12A) and the VA/VL complex (Fig. 12A, B) with some extending into VP (Fig. 12B). The labeling in Rt was observed in all cases analysed, having a similar position, irrespective of the origin

in PPC. A few fibers were labeled in CL, Re, Rh, and nucleus submedius (Sub, Fig. 12A-C). More caudally, labeling was also found in the anterior pretectal nucleus (AP, Fig. 12E, F). No labeling was seen in DLG (Fig. 12C-F).

Injections located more caudally in mPPC resulted in comparable distributions of labeling in the thalamus. A representative injection of BDA (13594B, Figs. 4B, 11, 13) covered mainly the deep layers, having its core in layer 5 (Fig. 11). As in the previous case, sparse labeling was found caudally in the lateral part of LDm (not illustrated). This labeling continued caudally and grew stronger in the ventrolateral part of LPmr where an additional patch was seen more medially (Fig. 13C-E). Labeling in Po shifted from a lateral position in rostral sections to a more medial position in sections positioned halfway along the rostrocaudal axis and ceasing in more caudal levels. Labeled fibers were present in LPl and AP (Fig. 13D, F), whereas no labeling was seen in VP or DLG (Fig. 13A-F). Comparing this result with the previous case leads us to conclude that the minor labeling in VP in the rostral case (Fig. 12B) is likely a result of the injection extending into S1.

*lPPC.* Most of the injections into lPPC involved the rostral part (Fig. 4B), with some showing a minor involvement of the rostrally adjacent somatosensory cortex. We also analyzed some injections located centrally in lPPC as well as a more caudally positioned injection. In all 9 cases, the pattern of thalamic labeling was comparable. In a case representative for injections in lPPC, the core of the PHA-L injection site was confined to layers 5 and 6 of the rostrolateral lPPC (13187P, Figs. 4B, 11, 14). The strongest labeling was seen dorsolaterally in Po, with a dense cluster of labeled fibers extending through several sections in the rostrocaudal direction (Fig. 14C-E). Contrasting injections in mPPC, the cluster of labeled

fibers after injection in lPPC maintained a dorsolateral position in Po along the rostrocaudal axis with a clear preference for caudal levels. Rostrally in the thalamus, labeling was found dorsally in the reticular nucleus and the VA/VL complex (Fig. 14A, B). A few labeled fibers were observed in CL and in Sub (Fig. 14C), even bilaterally. Similar to injections in mPPC, this injection also gave rise to some labeling caudal in LDm extending into rostral LPmr (Fig. 14C, D), but labeling was now positioned medially compared to the pattern that resulted from injections in mPPC. In more caudal sections, weak labeling was seen ventromedially in LPl (Fig. 14E, F). Scattered smooth labeled fibers were found in caudal VP and AP, but no labeling was observed in DLG (Fig. 14C-F).

One BDA injection was located caudomedially in lPPC (12948B, Figs. 4B, 11, 15), and yielded similar thalamic labeling patterns as the above described case 13187P. The injection site covered layers 3 through 6 (Fig. 11). The strongest cluster of labeled terminal axons was consistently found in dorsolateral Po extending several sections in the rostrocaudal direction (Fig. 15B-E). Sparse labeling was observed in the LDm/LPmr transition, VA/VL, VP, Sub, and AP, while labeled fibers were absent in DLG.

*PtP*. Six tracer injections were made in the part of posterior parietal cortex called PtP (Fig. 4B). Due to the narrow medial-lateral extent of PtP, all injections extended slightly into either V2L medially or S1 laterally. Nevertheless, the injections yielded similar patterns of labeled fibers in the thalamus. In one representative case, the PHA-L injection covered all layers of PtP while being centered in layers 5 and 6 and impinging on V2L (12906P, Figs. 4B, 11, 16). This injection yielded a thalamic labeling pattern similar to that observed following injections in lPPC described above. The most prominent labeling was seen dorsolaterally in the Po

complex, where a strong cluster of labeled fibers was found extending through several sections in the rostrocaudal extent (Fig. 16B-E). In addition to the lateral cluster a small, weaker cluster was observed dorsomedially in Po (Fig. 16C, D), with some fibers extending into the LDm/LPmr transition as well as into CL. Labeling was further present in the VA/VL complex (Fig. 16A) and Sub (not illustrated), and two small clusters of labeling were situated dorsally in Rt (Fig. 16A-C). A few fibers were seen extending into VP (Fig. 16C-E). Some labeling was found ventrally in LPl (Fig. 16E) in addition to the caudal extreme of LPmr (Fig. 16F), as well as in AP (not shown). No labeling was found in DLG. In another animal (12877B, Fig. 4B, labeling pattern not illustrated), BDA was injected in PtP slightly caudal and lateral to the above described injection, impinging on S1. In line with the first case, the strongest labeling was seen in dorsolateral Po, but a medial cluster was not observed. Relatively more labeled fibers were found in LD in this case, in addition to a restricted cluster of labeled fibers in VPm that was not seen in the first case.

*Injections in the primary somatosensory cortex*

The four injections in the dorsomedial S1 were located differently along the rostral-caudal and medial-lateral axes (Fig. 4B), but yielded comparable labeling patterns in the thalamus. One representative case had a BDA injection centered caudally in the hindlimb region of the primary somatosensory cortex (16082B, Figs. 4B, 11, 17). The core of the injection was located in layers 4 and 5, but the injection extended to all other layers (Fig. 11). The strongest labeling was found in VPl (Fig. 17B-D). There was also a small, dense cluster dorsally in Po (Fig. 17D). Some fibers were seen laterally in the LDm/LPmr transition (Fig. 17C, D), similar to what was observed in some of the PPC cases. There was focused labeling dorsally in Rt

and some labeling in the VA/VL complex (Fig. 17A). Caudally there was a distinct cluster of labeled fibers in AP (Fig. 17E, F). No labeling was found in DLG (Fig. 17D-F).

Nine injections were distributed in different portions of the barrel cortex (Fig. 4B), all resulting in similar labeling patterns. In a representative case, the PHA-L injection was positioned caudally in the barrel cortex, possibly with a minor extension into lateral portions of PPC (12551P, Figs. 4B, 11, 18). The injection site covered layers 2-5, having its core in layers 3 and 4 (Fig. 11). The labeling pattern closely resembled the pattern described above for the injection in the hindlimb area (Fig. 17), with some differences. The strongest labeling was now shifted to VPm (Fig. 18C-E). Labeling was also seen in Po, but the cluster was shifted more lateral and ventral compared to the previous case, and labeling resulting from the barrel cortex injection covered a larger area of the Po than was seen after the hindlimb area injection (Fig. 18C-E). The larger extent of labeling could be a result of the larger injection site (Fig. 11). Similar to the previous case, some labeling was found in Rt, the LDm/LPmr transition, and AP (Fig. 18B-D, F). No labeling was observed in DLG (Fig. 18E, F).

*Injections in the visual cortex*

*V1*. In total, 16 injections of anterograde tracers were distributed across primary and secondary visual cortices (Fig. 4B). In a single representative animal, we injected two tracers in the visual cortex (12951P and 12951B, Figs. 4B, 11, 19). Both injections were focused in the primary visual cortex but were offset from each other (Fig. 11). The PHA-L injection was positioned slightly more medial and caudal than the BDA injection. The PHA-L injection covered all layers, whereas the BDA injection had a core in layers 4 through 6, extending only somewhat into the superficial layers. The overall labeling pattern was similar for both

injections, though with some topographical variations, resulting in labeling that only marginally overlapped between the two cases (Fig. 19; the rostral BDA injection results are shown in green, while the caudal PHA-L resulting labeling is shown in magenta). Two dense bundles of fibers were seen coming in through the external medullary lamina (Fig. 19C, D), eventually terminating in DLG (Fig. 19E, F), where the strongest labeling was observed. The two bundles and clusters were clearly separated with minimal overlap. In LD, sparse labeling was found laterally in both cases (Fig. 19A-C). A few fibers were found in the medial parts of LD/LP (Fig. 19C). At more caudal thalamic levels, some fibers in the lateral LP were labeled (Fig. 19E), and a small but dense cluster of labeled fibers was seen in the caudal extreme of LPmr (Fig. 19F). Clustered but not very dense labeling was also observed dorsally in Po (Fig. 19B). The rostral BDA injection gave rise to a small cluster of labeled fibers in CL which was not seen in case of the more caudal PHA-L injection (Fig. 19C). Both injections resulted in labeling in the VA/VL complex, dorsally in Rt, and in Sub (Fig. 19A-C). In AP, fibers were seen passing through without terminating, while in the zona incerta, clear terminal labeling was observed, resulting from the rostral BDA injection (Fig. 19F). No labeling was seen in VP.

The second case we selected had combined tracer injections into primary and secondary visual cortices (14353B and 14353P, Figs. 4B, 11, 20). The BDA injection was centered in the primary visual cortex, covering layers 3 through 5 with some extension into layer 6 (Fig. 11). The labeling pattern (Fig. 20, visualized in green) was similar to that described above for both injections in primary visual cortex (case 12951), though with some variation. As in all other V1 cases, a dense bundle of labeled fibers was seen coming in through the external medullary lamina (Fig. 20C, D), giving rise to a large cluster of dense terminal labeling in DLG (Fig. 20E, F). Weak labeling was present in LDm (Fig. 20A, B) and a stronger labeled

cluster in LPmr was located medially (Fig. 20C, D), while more caudally, there was a labeled cluster laterally in LPmr (Fig. 20E). This is in contrast to case 12951 described above, where most labeling in LD and LP was seen in LDl and LPl. However, the small patch of labeled fibers in the caudal extreme of LPmr is consistent for all V1 injections and appears to overlap with the patch of labeled cells observed after injections of retrograde tracers in V1. Also similar to all other V1 cases, no labeling was found in VP (Fig. 20A-E), whereas AP contained sparsely labeled fibers (Fig. 20F).

*V2.* The accompanying PHA-L injection (14353P, Figs. 4B, 11; thalamic labeling in Fig. 20 visualized in magenta) was centered rostrally in the medial part of the secondary visual cortex with a core in layers 5 and 6, extending into layers 4 and 3 (Fig. 11). In contrast to the injections in primary visual cortex, we did not observe labeling in DLG (Fig. 20C-F). Strong labeling was found in LD and LP after injecting tracer into V2M, as for injections in V1. However, projections from V2M showed almost no overlap with those from V1. The projections from V2M were observed in medial and lateral subdivisions throughout LD and LP, while fibers originating in V1 in this case were situated mainly in the medial subdivision of these nuclei (Fig. 20A-E). Rostrally in LPmr, fibers from V1 were seen in the ventromedial portion, while projections from V2M terminated more dorsally (Fig. 20C-E). The patch of labeled fibers in caudal LPmr that was observed in all V1 cases was not found in the V2M case (Fig. 20E). In contrast, very notable in V2M cases, but not V1 cases, was a dense patch of labeled fibers ventrally in LPl, as well as a stripe of labeled fibers in the same nucleus bordering the intramedullary thalamic area lining the medial wall of DLG (Fig. 20E). In Po, fibers from V2M were wedged in between two smaller clusters of fibers from V1 (Fig. 20B). A bundle of fibers from both cortical areas was seen to pass through VA/VL ending in Sub (Fig. 20A, B).

In one animal, BDA was injected rostrally in V2L (20546B, Figs. 4B, 11; thalamic labeling not illustrated). The injection site extended across layers 3-6, with the densest labeling in layer 5 (Fig. 11). The thalamic labeling pattern was strikingly similar to the PHA-L injection in V2M described above. In rostral sections, labeled fibers were found to pass through VA/VL ending in Sub. A small cluster of labeled fibers was seen in lateral LD. In LP, a dense cluster of labeled fibers was observed ventrally in LPl, in caudal sections this cluster was situated close to DLG and thus slightly more lateral than the cluster observed after injection of tracer into V2M. In addition, labeled fibers were found in LPmr at a mid-dorsoventral level. Caudally, a stripe of labeled fibers was seen in LPl, bordering the intramedullary thalamic area. Different from the V2M case described here, the V2L case had labeled fibers also in the ventrolateral geniculate nucleus (VLG). However, these fibers appeared smooth and did not branch, indicating they were not terminating fibers.

## Discussion

### Topography and nomenclature

In this study, we used a combination of cyto- and chemoarchitectonic criteria in addition to patterns of thalamic connectivity to differentiate between areas in the dorsal caudal cortex of the rat brain, including parietal and occipital domains. The aim of the present study was to define the posterior parietal cortex and to differentiate it from the rostrally adjacent somatosensory cortex and caudally adjacent visual domains. Delineation of the caudal cortex of the rat has previously been attempted based on cyto-, chemo- and myeloarchitecture, physiological properties of neurons, and connectivity with cortical or subcortical areas. Relevant for this study is the consensus that the border between the posterior parietal cortex

and the visual cortex has been particularly difficult to establish. Although our findings are in line with previous studies, here we provide a complete correlative assessment of the architectonics and corticothalamic connectivity of the posterior parietal cortex and its adjacent cortical areas (for previous studies, see for instance Price and Webster, 1972; Hughes, 1977; Saporta and Kruger, 1977; Wise and Jones, 1977; Perry, 1980; Fabri and Burton, 1991; Chandler et al., 1992; Reep et al., 1994; Kamishina et al., 2009; Wilber et al., 2015).

In our study, primary somatosensory and primary visual cortices were easily discerned based on their prominent granular layer 4 and cell sparse superficial layer 5 which has been described in earlier studies (Krieg, 1946a; Welker, 1971; Palomero-Gallagher and Zilles, 2004). The region between the two primary cortices, together with areas medial and lateral to the primary visual cortex, form a heterogenous region of cortical areas that in general have a more diffuse lamination and a higher cell density in layer 5 than the primary areas. While we have not studied the physiological properties of cells in these areas, based on architectural features and thalamic connectivity we conclude that there is indeed a posterior parietal cortex situated between S1 and V1/V2. Furthermore, we propose that PPC can be reliably subdivided into two main areas, a dorsal and ventral limb (Burwell and Amaral, 1998). For the dorsal limb we maintain the name posterior parietal cortex (PPC) as it has been widely used in functional studies of the area (see for instance Nitz, 2012; Whitlock et al., 2012). The dorsal limb can further be subdivided into medial (mPPC) and lateral (lPPC) components, referred to as medial (MPtA) and lateral parietal association (LPtA) cortex in a widely used atlas of the rat brain (Paxinos and Watson, 2007). On the other hand, we refer to the ventral limb as the posterior part of parietal cortex (PtP) following the nomenclature used in this atlas. In our hands, neither architectonic criteria, nor thalamic connectivity were sufficiently reliable to further subdivide PtP. In this, we differ from some other authors (Palomero-Gallagher and

Zilles, 2004; Paxinos and Watson, 2007). We further deviate from the description by the latter authors of the medial border of mPPC. In their delineations, mPPC borders M2 at rostral levels and RSC at caudal levels, in line with another study (Reep et al., 1994). While we agree with the mPPC/M2 border at rostral levels, we found that a narrow, rostral extension of V2M is wedged between mPPC and RSC at caudal levels and in our data, mPPC does not border RSC. It is possible that the complicated distinction between V2M and mPPC has led previous authors to draw the medial border of mPPC at the lateral limit of RSC. Nevertheless, the resulting delineations of the three main domains of PPC coincide to a large extent with the delineations applied in the above mentioned atlas (Paxinos and Watson, 2007). The observed variations in thalamic connectivity corroborated all architectonic borders, showing that individual cortical areas are differently connected with specific sets of thalamic nuclei.

Thalamic connectivity

Our conclusions about thalamic connectivity, summarized in Figure 21, are mainly based on results of injections of anterograde tracers in PPC, since these in general were smaller and hence more likely to be confined to one area than injections of retrograde tracers. Moreover, we have cases with anterograde but not retrograde tracer injections in areas PtP and V2L. It is however important to point out that our retrograde results overall support the anterograde data, since both yield labeling in corresponding thalamic domains. This validates the notion that thalamocortical and corticothalamic projections to a large degree are reciprocal (Deschenes et al., 1998). Our main findings are: (1) mPPC is reciprocally connected with ventrolateral LPmr; (2) lPPC is reciprocally connected with the dorsal portion of Po; (3) PtP projects more ventral in Po; (4) S1 is reciprocally and topographically connected with VP and Po; (5) V2M is reciprocally connected with LPl, mid-dorsoventral LPmr, and LD; (6) V2L

thalamic projections are similar to V2M thalamic projections and reach mainly LPl and mid-dorsoventral LPmr; (7) V1 is reciprocally connected with DLG and a specific patch of cells caudally in LPmr.

Results from injections of retrograde tracers indicate that mPPC receives input from LP, mainly from the ventral rostromedial part. However, in one case with a retrograde tracer injection in caudal mPPC, we observed labeled cells in lateral LP as well as more dorsally within LPmr. This is likely a result of the injection site extending into the caudally adjacent V2M. Indeed, our data show that V2M receives thalamic input that originates throughout the lateral-to-medial extent of LP. Based on the concept of reciprocity (Deschenes et al., 1998), our anterograde data are in line with this interpretation, indicating that mPPC preferentially projects to medial and central parts of LP. Our retrograde data indicate that lPPC receives inputs from Po as well as from LP and even from DLG. The labeling in the latter two nuclei is likely due to our injections being placed close to and involving V1, which receives input from these two thalamic nuclei. Applying the principle of reciprocity validates this interpretation, since our anterograde data show that lPPC projections to Po are substantially stronger than those to LP, and we did not observe any projections from lPPC to DLG. Our interpretation is in accordance with anterograde tracing data showing that dorsal Po preferentially projects to lPPC and PtP, while LPmr sends heavier projections to mPPC than lPPC (Kamishina et al., 2009). Our results are further supported by a retrograde tracing study in which a similar pattern of LP and Po projections to respectively mPPC and lPPC was observed (Reep et al., 1994), as well as a recent retrograde tracing study where lPPC was found to receive a higher proportion of input from Po than mPPC (Wilber et al., 2015). However, the latter study also observed that lPPC received a higher proportion of input from LPmr than mPPC, which is contrary to our findings. It should be noted that these authors grouped tracer injections into

lPPC and area V2ML together, and the discrepancy can be explained by V2M receiving input from LPmr as seen in our data. We thus conclude that mPPC and lPPC, two areas that are architectonically differentiable, also differ in their main thalamic connectivity, with mPPC being connected preferentially with LPmr and lPPC preferentially with Po.

Information about the thalamic connections of the parietal area PtP is sparse. Although we had six successful injections of anterograde tracers into PtP, all of them impinged on surrounding cortical areas. Based on the obtained results, showing that PtP projects densely to a specific portion of Po, we conclude that PtP is similar to lPPC in this respect. It should be mentioned that PtP appears to project slightly more ventral in Po than lPPC, indicating that topographic differences in the projection patterns may exist. Taking into account that thalamocortical and corticothalamic connections overall are reciprocal, our observations are in line with an anterograde tracing study in which a projection from Po to PtP was described (Kamishina et al., 2009). Although lPPC and PtP have comparable thalamic connectivity, they can be differentiated based on architectural features, as PtP contains a less densely packed layer 5 and a lightly stained layer 3/4 compared to lPPC.

Previous studies have consistently reported reciprocal connections of the rat PPC with LD (Ryszka and Heger, 1979; Reep et al., 1994; Kamishina et al., 2009; Wilber et al., 2015). In contrast, in our data we found reciprocal connectivity between LD and mPPC or lPPC to be sparse. Regarding PtP, our data only indicated weak projections to LD. On the other hand, our data show moderate reciprocal connections between LD and V2M and sparser reciprocal connections between LD and V1, in addition to projections from V2L to LD. It is thus likely that the claimed reciprocal connections between LD and PPC partially reflect the connectivity

of visual cortical areas. This leads us to the conclusion that the entirety of PPC is only weakly connected with LD.

Our conclusion that thalamic projections to V2M originated mainly in LP and LD, but not in Po is in line with a previous study (Reep et al., 1994). Another study found that dense projections to V2M originate in LPl (Kamishina et al., 2009), which is coherent with our findings, although these authors also described sparser LPl projections to PPC which was not seen in our retrograde data. Further, our observation that V2L projects to LPl is in agreement with previous findings (Coogan and Burkhalter, 1993) but we did not see projections to DLG which were described by these authors. Our data contradict a recent study, which failed to find significant differences in input patterns between PPC and V2M (Wilber et al., 2015). These authors observed that both cortical areas receive strong input from LPmr, but did not consider the location of the labeled cells within the nucleus. In our dataset, it is clear that the two cortical areas are connected with complementary populations of LPmr neurons. Moreover, our retrograde and anterograde tracer data indicate that V2M has stronger connections with LPl than LPmr, while LPl connections were only occasionally observed in PPC cases. Our data are further in conflict with a retrograde tracing study reporting that projections to rostral portions of V2 originated primarily in Po, while those to caudal V2 arose mainly from LP (Sanderson et al., 1991). Our injections of retrograde and anterograde tracers centered rostrally in V2M failed to produce a high proportion of labeling in Po. Unfortunately, not all injection sites of the above mentioned study were shown and it is possible that the injections in rostral V2 involved portions of PPC, in which case the results would be consistent with our data.

The PPC is easily distinguished from the rostrally adjacent S1 areas based on architectonic criteria, but also differs from S1 with respect to its thalamic connections. The body surface of the rat is strictly topographically represented in the ventral posterior nucleus of the thalamus (Emmers, 1965) and the primary somatosensory cortex of the rat (Welker, 1971). Information from the face is represented medially in VP and laterally in the cortex, while information from the limbs and trunk of the body is represented laterally in VP and medially in the cortex (Price and Webster, 1972; Saporta and Kruger, 1977; Wise and Jones, 1977; Nothias et al., 1988; Fabri and Burton, 1991). These findings are supported by our data where retrograde and anterograde tracer injections medially in S1 (trunk and hindlimb representing areas, respectively, according to Paxinos and Watson, 2007) labeled projections to and from lateral VP and dorsal Po, close to LP. The laterally situated barrel cortex is also connected with VP and Po, but with a different population within those two nuclei. In VP, the labeling was dense in the medial portion, while in Po it was located more ventrally and thus closer to VPm rather than to LP. Although not connected to VP, lateral portions of the posterior parietal cortex, like S1, are connected with Po (our data as well as Reep et al., 1994; Kamishina et al., 2009). Thus, lPPC and medial S1, both situated dorsally in the cortex, are reciprocally connected with dorsal Po, although small differences are apparent, as lPPC projections to Po terminate slightly more lateral than S1 projections. The caudolaterally situated PtP and barrel cortex both project more ventrally in Po, with PtP projections spreading over a larger portion than those from the barrel cortex. mPPC is only sparsely connected with Po and is thus easily discerned from somatosensory cortex based on thalamic connectivity.

As mentioned previously, while PPC is readily distinguished from the adjacent primary cortices S1 and V1 based on architectonic criteria, the anatomical distinction between PPC and the caudally adjacent secondary visual cortices has long been debated in the literature. In

our material, the area we have denoted as mPPC appears less laminated than V2M in Nissl stained sections, lPPC mainly borders V1 which is characterized by its prominent granular layer 4, while PtP has weakly stained cells in layer 3/4 compared to adjacent areas. Thus, architectural criteria distinguish PPC from its surrounding cortices. Moreover, our tracing data suggest that the thalamic projections of PPC and the surrounding cortices differ, further arguing that PPC should be recognized as a distinct cortical region. In sum, PPC projects strongly to LPmr and Po nuclei of the thalamus, in particular, mPPC projects to LPmr while lPPC and PtP project to Po. Although V2M and V2L share projections to LPmr, their projections terminate more strongly in LPl than in LPmr, and within the latter nucleus mPPC and V2 projections show a complementary distribution. While mPPC projections target a ventrolateral portion of LPmr, V2M and V2L project to a mid-dorsoventral portion. Further, projections from PPC subregions to LPl are sparse or non-existent, and we therefore consider the LPl projection to be specific for secondary visual areas. In addition, we found only very sparse projections of PPC subregions to LD whereas moderate projections to this nucleus were consistently seen after tracer injections in primary and secondary visual cortices. mPPC thus projects to a ventrolateral region within LPmr which lacks input from visual cortices, while it does not project to the visually targeted LPl and LD. We further report that lPPC and PtP projections target Po rather than LPmr, and visual cortices only weakly project to Po, reinforcing the distinction between PPC and its caudally adjacent areas. The projections from lPPC and PtP to Po overlap to some extent with those from the somatosensory domain although PPC projections extend over a larger area than those from S1. Moreover, PPC lacks projections to the primary somatosensory VP nucleus, distinguishing it from the somatosensory cortical domain. In conclusion, PPC as a whole can be distinguished from its adjacent somatosensory and visual domains in terms of both architecture and thalamic connections.

Comparative considerations

*Homology of thalamic nuclei*

In general, the PPC of cats and monkeys, like in rats, is reciprocally connected with associative thalamic nuclei. More specifically, PPC is connected with portions of the LP-pulvinar complex in monkeys, and with portions of the LP-pulvinar complex and the posterior group in cats. Comparing thalamic connectivity across species is complicated due to highly variable nomenclature (Jones, 2007). However, thalamic nuclei connected with PPC in monkeys, cats, and rats share some connectional similarities. For instance, the anterior pulvinar nucleus in monkeys and the posterior medial nucleus in cats both receive spinal and trigeminal inputs and are connected with somatosensory cortices (Jones, 2007). The rat homology of these nuclei might be the posterior complex (Po), which receives spinal and trigeminal input, and is connected with the somatosensory cortex (Vertes et al., 2014). The LP nucleus of the monkey and the lateral portion of the LP nucleus in the cat have ill-defined subcortical input, and in both species these nuclei are interconnected with areas 5 and 7 (Jones, 2007). The medial pulvinar nucleus in the monkey and the medial portion of the LP nucleus of the cat have minor inputs from the superior colliculus and are connected with widespread areas of the cortex, including PPC, visual areas, and temporal regions. Projections to the various cortical areas are thought to originate in different subpopulations within the nuclei (Jones, 2007). In the rat, LP has distinguishable architectonically defined subdivisions (Paxinos and Watson, 2007), but to our knowledge no studies have tried to separate these subdivisions functionally. However, connections of LP with PPC and visual areas exist, and these seem to arise from different subpopulations within these nuclei (Reep et al., 1994; Vertes et al., 2014; our data). This suggests that at least portions of LP in rat may be

homologous to LP and medial pulvinar nuclei in monkeys, and to the lateral and medial LP in cats. Thus, PPC in rats appears to be connected with thalamic nuclei that are comparable to those connected with PPC in cats and monkeys.

*Homology of cortical areas*

The PPC of the rat was first described as area 7 based on its position between the somatosensory and visual cortices, similar to area 7 in higher species (Krieg, 1946b). Here, we show that PPC in rats clearly differs from the caudally adjacent visual cortex with respect to architecture and thalamic connectivity. Also in monkeys and cats, connections of PPC with LP and pulvinar nuclei do not seem to overlap (or do so minimally) with the thalamic connections of visual cortical areas (Robertson and Cunningham, 1981; Gutierrez and Cusick, 1997; Adams et al., 2000; Jones, 2007). Thus, in rats, cats, and monkeys, PPC can be differentiated from visual cortices based on the thalamic connectivity pattern.

The rostral portion of area 7 in monkeys is connected primarily with the anterior pulvinar nucleus, while the more caudal portion is primarily connected with the medial pulvinar nucleus (De Vito and Simmons, 1976; Baleydier and Mauguiere, 1977; Divac et al., 1977; Mesulam et al., 1977; Kasdon and Jacobson, 1978; Pearson et al., 1978; Asanuma et al., 1985; Yeterian and Pandya, 1985; Baleydier and Mauguiere, 1987; Schmahmann and Pandya, 1990; Cavada et al., 1995; Gutierrez et al., 2000). Within these studies, descriptions of connections between area 7 and LP nucleus vary. In the cat, most studies emphasize the strong connections of area 7 with LP and pulvinar nuclei, while connections with the posterior medial nucleus appear to be minor. Moreover, some studies describe a gradient of connections where rostral area 7 is connected with the LP nucleus while caudal area 7 are preferentially

connected with the rostral part of the pulvinar nucleus (Robertson and Rinvik, 1973; Mizuno et al., 1975; Robertson, 1976; 1977; Berson and Graybiel, 1978; Robertson and Cunningham, 1981; Olson and Lawler, 1987). The rostral-caudal gradient of area 7 thalamic connections in monkeys and cats may be related to the lateral-medial gradient of PPC thalamic connections in rats, where PtP and lPPC are connected with the posterior complex, which is homolog to the anterior pulvinar in monkeys and posterior medial nucleus in cats. On the other hand, rat mPPC is connected with LP, homolog to the LP-pulvinar complex in monkeys and cats.

Whether or not the rat PPC contains an area 5, as in cats and monkeys, is difficult to establish based on architectural features and thalamic connections. In monkeys, area 5 generally appears cytoarchitectonically more homogenous than area 7, which from rostral to caudal displays a clearer demarcation of layers 2, 4, and 6 (Pandya and Seltzer, 1982). In cats, a decrease in the size of layer 5 pyramidal neurons has been noted from rostral area 5 to caudal area 7 (Robertson and Cunningham, 1981; Avendaño et al., 1985). In our material, we did not detect a rostrocaudal gradient in the cytoarchtitectural features of PPC. On the other hand, cell density in layer 5 decreased from medial to lateral portions of PPC, giving an impression of increased lamination. However, we did not investigate possible differences in the size of neurons in layers 3 or 5 between subareas. In cats and monkeys, thalamic connections of area 5 appear to be similar to area 7 connections, namely with LP and anterior pulvinar nuclei in monkeys, and LP and posterior complex in cats (Graybiel, 1972; Robertson and Rinvik, 1973; De Vito and Simmons, 1976; Robertson, 1977; Graybiel and Berson, 1980; Robertson and Cunningham, 1981; Avendaño et al., 1985; Yeterian and Pandya, 1985; Schmahmann and Pandya, 1990; Amino et al., 2001; Cappe et al., 2007). Thus, architecture and thalamic connectivity alone provide insufficient information to decide whether or not area 5 exists in rats, and more detailed anatomical and functional studies are required.

Functional considerations

In studying the function of a cortical area, it is crucial that the area in question is well defined. As seen throughout this study, the distinction between the posterior parietal cortex and the visual domain has been difficult to establish in the rat brain. Most studies found the primary visual cortex to be easily identified by architectonic and physiological criteria. In contrast, the borders of the surrounding areas are debated. In some studies, regions medial, rostral, and lateral to the primary visual cortex in rats were considered to consist of one continuous area, whereas other authors suggested that they are subdivided into several areas, each of which are retinotopically organized as well as intrinsically connected in a hierarchical manner (Montero et al., 1973a,b; Espinoza and Thomas, 1983; Thomas and Espinoza, 1987; Coogan and Burkhalter, 1990, 1993; Sanderson et al., 1991; Montero, 1993; Reep et al., 1994; Palomero-Gallagher and Zilles, 2004). Recording experiments in parietal and occipital cortices of rats, mice, cats, and monkeys showed that PPC neurons had visual receptive fields, but these were in general larger, less specific and of a more associative nature than receptive fields observed in visual cortical areas (Montero et al., 1973b; Robertson, 1976; Blatt et al., 1990; Wang and Burkhalter, 2007). However, *in vivo* recording studies have found populations of neurons with similar functions across PPC and V2M (Nakamura, 1999; Wilber et al., 2014). On the other hand, bimodal neurons that respond to visual and somatosensory stimulation appear to be confined to PPC (Wagor et al., 1980; Toldi et al., 1986), this points to a distinction between posterior parietal and visual cortices as discussed previously.

In monkeys, functional specialization of subregions of PPC is well established (for review, see for instance Rawley and Constantinidis, 2009). We have found that the three main

subregions of PPC in rats, mPPC, lPPC and PtP, show variations in their architecture and thalamic connections, hinting towards functional specializations. Aside from the above mentioned variations in visual receptive field sizes (Montero et al., 1973b), few functional studies of PPC in rats have investigated in depth possible differences between the three subregions. Lesion studies typically assessed lesions of the entire PPC (Kolb and Walkey, 1987; DiMattia and Kesner, 1988; Save and Moghaddam, 1996; Save and Poucet, 2000). Most recording experiments in freely behaving animals thus far have studied neuronal activity only in the medial portion of PPC (Chen et al., 1994a,b; Nitz, 2006, 2012; Whitlock et al., 2012). To our knowledge, only one study reported a few recordings in lPPC, and no systematic difference was found regarding the function of lPPC versus mPPC (Wilber et al., 2014). Within mPPC, a possible rostrocaudal topography in function has been described in that cells located caudally in mPPC have head directional properties (Chen et al., 1994a, b), whereas such properties were not described for cells more rostrally in mPPC (Nitz, 2006). However, in later studies cells were recorded throughout mPPC and no functional topography was found within this area (Nitz, 2012; Whitlock et al., 2012). The latter observations support our notion that no topographical differences are apparent within mPPC regarding thalamic connectivity.

In view of the differences in thalamic connectivity between the three main subregions, mPPC, lPPC and PtP, we would expect functional differentiations between these, comparable to functional differences within monkey and cat PPC (Robertson, 1976; Cavada and Goldman-Rakic, 1993; Rawley and Constantinidis, 2009). It would be particularly meaningful to complement studies on variations in sensory processing between these three main subdivisions with detailed analyses of potential differences in cognitive processes. In this respect, the reciprocal connection of mPPC with LPmr may indicate that this PPC subdivision

processes visuospatial information since LPmr is strongly connected with other cortical and subcortical regions involved in such processing (Reep et al., 1994; Reep and Corwin, 1999; Conte et al., 2008; Kamishina et al., 2008, 2009). Moreover, lesions of several LPmr connected regions, including PPC, result in deficits in visuospatial processing such as neglect (Reep et al., 2004). As mentioned previously, the apparent strict topographical organization of LPmr connections suggest that this nucleus may be subdivided in distinct anatomical domains (Reep et al., 1994; Vertes et al., 2014; our data), but to our knowledge, no studies have investigated possible topographies in the functional properties of cells within LPmr. Although the evidence is strong that mPPC processes visuospatial information, neurons in this area have been found to respond to auditory cues as well as somatosensory and visual stimuli (Wagor et al., 1980; Toldi et al., 1986; Nakamura, 1999). The connections of lPPC and PtP with Po may hint to a role in processing of proprioceptive information, since Po is also strongly associated with somatosensory cortices (Vertes et al., 2014; our data). Since lPPC is reciprocally connected with dorsal Po, which is also connected with trunk and limb representing areas of S1, whereas PtP projects more ventrally in Po close to the domain where information from the face and head is processed, we suggest that lPPC and PtP process proprioceptive information about the body and head, respectively. In contrast to mPPC, neurons in lPPC and PtP show bimodal responses to somatosensory and visual stimuli but not to auditory stimuli (Wagor et al., 1980; Toldi et al., 1986). Combined descriptions of differences in cortical and subcortical connectivity between PPC subdivisions could help to understand a possible functional diversity within PPC and the here presented delineations and specifications of connectivity with thalamic nuclei will facilitate detailed studies on the role of the subdivisions of PPC in the rat as diverse, higher order associative cortical areas, comparable to those described in the primate.

**Acknowledgments:** We greatly appreciate the excellent technical assistance of Bruno Monterotti and Paulo Girão in sectioning and histological processing of parts of the material. We further thank Hanna Haaland Sømme and Karoline Hovde for providing some of the experimental cases.

**Conflict of interest:** The authors report no conflicts of interest.

**Role of authors:** All authors had full access to all the data in the study and take responsibility for the integrity of the data and the accuracy of the data analysis. Study concept and design: MPW. Acquisition of data: GMO. Analysis and interpretation of the data: GMO and MPW. Drafting of the manuscript: GMO. Critical revision of the manuscript for important intellectual content: MPW. Obtained funding: MPW. Study supervision: MPW.

## Literature cited

Adams MM, Hof PR, Gattass R, Webster MJ, Ungerleider LG. 2000. Visual cortical projections and chemoarchitecture of macaque monkey pulvinar. J Comp Neurol 419(3):377-393.

Amino Y, Kyuhou S, Matsuzaki R, Gemba H. 2001. Cerebello-thalamo-cortical projections to the posterior parietal cortex in the macaque monkey. Neurosci Lett 309(1):29-32.

Asanuma C, Andersen RA, Cowan WM. 1985. The thalamic relations of the caudal inferior parietal lobule and the lateral prefrontal cortex in monkeys: divergent cortical projections from cell clusters in the medial pulvinar nucleus. J Comp Neurol 241(3):357-381.

Avendaño C, Rausell E, Reinoso-Suarez F. 1985. Thalamic projections to areas 5a and 5b of the parietal cortex in the cat: a retrograde horseradish peroxidase study. J Neurosci 5(6):1446-1470.

Baleydier C, Mauguiere F. 1977. Pulvinar-latero posterior afferents to cortical area 7 in monkeys demonstrated by horseradish peroxidase tracing technique. Exp Brain Res 27(5):501-507.

Baleydier C, Mauguiere F. 1987. Network organization of the connectivity between parietal area 7, posterior cingulate cortex and medial pulvinar nucleus: a double fluorescent tracer study in monkey. Exp Brain Res 66(2):385-393.

Berson DM, Graybiel AM. 1978. Parallel thalamic zones in the LP-pulvinar complex of the cat identified by their afferent and efferent connections. Brain Res 147(1):139-148.

Blatt GJ, Andersen RA, Stoner GR. 1990. Visual receptive field organization and cortico-cortical connections of the lateral intraparietal area (area LIP) in the macaque. J Comp Neurol 299(4):421-445.

Burette AC, Strehler EE, Weinberg RJ. 2009. "Fast" plasma membrane calcium pump PMCA2a concentrates in GABAergic terminals in the adult rat brain. J Comp Neurol 512(4):500-513.

Burwell RD, Amaral DG. 1998. Cortical afferents of the perirhinal, postrhinal, and entorhinal cortices of the rat. J Comp Neurol 398(2):179-205.

Cappe C, Morel A, Rouiller EM. 2007. Thalamocortical and the dual pattern of corticothalamic projections of the posterior parietal cortex in macaque monkeys. Neuroscience 146(3):1371-1387.

Cavada C, Company T, Hernandez-Gonzalez A, Reinoso-Suarez F. 1995. Acetylcholinesterase histochemistry in the macaque thalamus reveals territories

selectively connected to frontal, parietal and temporal association cortices. J Chem Neuroanat 8(4):245-257.

Cavada C, Goldman-Rakic PS. 1993. Multiple visual areas in the posterior parietal cortex of primates. Prog Brain Res 95:123-137.

Cerkevich CM, Qi HX, Kaas JH. 2013. Thalamic input to representations of the teeth, tongue, and face in somatosensory area 3b of macaque monkeys. J Comp Neurol 521(17):3954-3971.

Chandler HC, King V, Corwin JV, Reep RL. 1992. Thalamocortical connections of rat posterior parietal cortex. Neurosci Lett 143(1-2):237-242.

Chen LL, Lin LH, Barnes CA, McNaughton BL. 1994a. Head-direction cells in the rat posterior cortex. II. Contributions of visual and ideothetic information to the directional firing. Exp Brain Res 101(1):24-34.

Chen LL, Lin LH, Green EJ, Barnes CA, McNaughton BL. 1994b. Head-direction cells in the rat posterior cortex. I. Anatomical distribution and behavioral modulation. Exp Brain Res 101(1):8-23.

Conte WL, Kamishina H, Corwin JV, Reep RL. 2008. Topography in the projections of lateral posterior thalamus with cingulate and medial agranular cortex in relation to circuitry for directed attention and neglect. Brain Res 1240:87-95.

Coogan TA, Burkhalter A. 1990. Conserved patterns of cortico-cortical connections define areal hierarchy in rat visual cortex. Exp Brain Res 80(1):49-53.

Coogan TA, Burkhalter A. 1993. Hierarchical organization of areas in rat visual cortex. J Neurosci 13(9):3749-3772.

De Vito JL, Simmons DM. 1976. Some connections of the posterior thalamus in monkey. Exp Neurol 51(2):347-362.

Deschenes M, Veinante P, Zhang ZW. 1998. The organization of corticothalamic projections: reciprocity versus parity. Brain Res Brain Res Rev 28(3):286-308.

DiMattia BV, Kesner RP. 1988. Role of the posterior parietal association cortex in the processing of spatial event information. Behav Neurosci 102(3):397-403.

Ding JD, Weinberg RJ. 2007. Distribution of soluble guanylyl cyclase in rat retina. J Comp Neurol 500(4):734-745.

Divac I, Lavail JH, Rakic P, Winston KR. 1977. Heterogeneous afferents to the inferior parietal lobule of the rhesus monkey revealed by the retrograde transport method. Brain Res 123(2):197-207.

Duttaroy A, Gomeza J, Gan JW, Siddiqui N, Basile AS, Harman WD, Smith PL, Felder CC, Levey AI, Wess J. 2002. Evaluation of muscarinic agonist-induced analgesia in muscarinic acetylcholine receptor knockout mice. Molecular pharmacology 62(5):1084-1093.

Emmers R. 1965. Organization of the first and the second somesthetic regions (SI and SII) in the rat thalamus. J Comp Neurol 124:215-227.

Espinoza SG, Thomas HC. 1983. Retinotopic organization of striate and extrastriate visual cortex in the hooded rat. Brain Res 272(1):137-144.

Fabri M, Burton H. 1991. Topography of connections between primary somatosensory cortex and posterior complex in rat: a multiple fluorescent tracer study. Brain Res 538(2):351-357.

Gray DT, Engle JR, Rudolph ML, Recanzone GH. 2014. Regional and age-related differences in GAD67 expression of parvalbumin- and calbindin-expressing neurons in the rhesus macaque auditory midbrain and brainstem. J Comp Neurol 522(18):4074-4084.

Graybiel AM. 1972. Some ascending connections of the pulvinar and nucleus lateralis posterior of the thalamus in the cat. Brain Res 44(1):99-125.

Graybiel AM, Berson DM. 1980. Histochemical identification and afferent connections of subdivisions in the lateralis posterior-pulvinar complex and related thalamic nuclei in the cat. Neuroscience 5(7):1175-1238.

Gutierrez C, Cola MG, Seltzer B, Cusick C. 2000. Neurochemical and connectional organization of the dorsal pulvinar complex in monkeys. J Comp Neurol 419(1):61-86.

Gutierrez C, Cusick CG. 1997. Area V1 in macaque monkeys projects to multiple histochemically defined subdivisions of the inferior pulvinar complex. Brain Res 765(2):349-356.

Hackney CM, Mahendrasingam S, Penn A, Fettiplace R. 2005. The concentrations of calcium buffering proteins in mammalian cochlear hair cells. J Neurosci 25(34):7867-7875.

Hughes HC. 1977. Anatomical and neurobehavioral investigations concerning the thalamo-cortical organization of the rat's visual system. J Comp Neurol 175(3):311-336.

Jones EG. 2007. The thalamus. Cambridge: Cambridge University Press. 2 b. : ill. p.

Kamishina H, Conte WL, Patel SS, Tai RJ, Corwin JV, Reep RL. 2009. Cortical connections of the rat lateral posterior thalamic nucleus. Brain Res 1264:39-56.

Kamishina H, Yurcisin GH, Corwin JV, Reep RL. 2008. Striatal projections from the rat lateral posterior thalamic nucleus. Brain Res 1204:24-39.

Kasdon DL, Jacobson S. 1978. The thalamic afferents to the inferior parietal lobule of the rhesus monkey. J Comp Neurol 177(4):685-706.

King VR, Corwin JV. 1993. Comparisons of hemi-inattention produced by unilateral lesions of the posterior parietal cortex or medial agranular prefrontal cortex in rats: neglect, extinction, and the role of stimulus distance. Behav Brain Res 54(2):117-131.

Kolb B, Walkey J. 1987. Behavioural and anatomical studies of the posterior parietal cortex in the rat. Behav Brain Res 23(2):127-145.

Krieg WJ. 1946a. Connections of the cerebral cortex; the albino rat; structure of the cortical areas. J Comp Neurol 84:277-323.

Krieg WJ. 1946b. Connections of the cerebral cortex; the albino rat; topography of the cortical areas. J Comp Neurol 84:221-275.

Lashley KS. 1941. Thalamo-cortical connections of the rat's brain J Comp Neurol 75(1):55.

Levey AI, Edmunds SM, Hersch SM, Wiley RG, Heilman CJ. 1995. Light and electron microscopic study of m2 muscarinic acetylcholine receptor in the basal forebrain of the rat. J Comp Neurol 351(3):339-356.

Levey AI, Kitt CA, Simonds WF, Price DL, Brann MR. 1991. Identification and localization of muscarinic acetylcholine receptor proteins in brain with subtype-specific antibodies. J Neurosci 11(10):3218-3226.

Levey AI, Stormann TM, Brann MR. 1990. Bacterial expression of human muscarinic receptor fusion proteins and generation of subtype-specific antisera. FEBS letters 275(1-2):65-69.

Mesulam MM, Van Hoesen GW, Pandya DN, Geschwind N. 1977. Limbic and sensory connections of the inferior parietal lobule (area PG) in the rhesus monkey: a study with a new method for horseradish peroxidase histochemistry. Brain Res 136(3):393-414.

Miller MW, Vogt BA. 1984. Direct connections of rat visual cortex with sensory, motor, and association cortices. J Comp Neurol 226(2):184-202.

Mizuno N, Konishi A, Sato M, Kawaguchi S, Yamamoto T. 1975. Thalamic afferents to the rostral portions of the middle suprasylvian gyrus in the cat. Exp Neurol 48(1):79-87.

Montero VM. 1993. Retinotopy of cortical connections between the striate cortex and extrastriate visual areas in the rat. Exp Brain Res 94(1):1-15.

Montero VM, Bravo H, Fernandez V. 1973a. Striate-peristriate cortico-cortical connections in the albino and gray rat. Brain Res 53(1):202-207.

Montero VM, Rojas A, Torrealba F. 1973b. Retinotopic organization of striate and peristriate visual cortex in the albino rat. Brain Res 53(1):197-201.

Nakamura K. 1999. Auditory spatial discriminatory and mnemonic neurons in rat posterior parietal cortex. J Neurophysiol 82(5):2503-2517.

Nitz DA. 2006. Tracking route progression in the posterior parietal cortex. Neuron 49(5):747-756.

Nitz DA. 2012. Spaces within spaces: rat parietal cortex neurons register position across three reference frames. Nat Neurosci 15(10):1365-1367.

Nothias F, Peschanski M, Besson JM. 1988. Somatotopic reciprocal connections between the somatosensory cortex and the thalamic Po nucleus in the rat. Brain Res 447(1):169-174.

Olson CR, Lawler K. 1987. Cortical and subcortical afferent connections of a posterior division of feline area 7 (area 7p). J Comp Neurol 259(1):13-30.

Palomero-Gallagher N, Zilles K. 2004. Isocortex. In: Paxinos G, ed. The Rat Nervous system. 3rd ed. San Diego, CA: Elsevier. p 729-757.

Pandya DN, Seltzer B. 1982. Intrinsic connections and architectonics of posterior parietal cortex in the rhesus monkey. J Comp Neurol 204(2):196-210.

Paxinos G, Watson C. 2007. The rat brain in stereotaxic coordinates. Amsterdam: Elsevier.

Pearson RC, Brodal P, Powell TP. 1978. The projection of the thalamus upon the parietal lobe in the monkey. Brain Res 144(1):143-148.

Perry VH. 1980. A tectocortical visual pathway in the rat. Neuroscience 5(5):915-927.

Price TR, Webster KE. 1972. The cortico-thalamic projection from the primary somatosensory cortex of the rat. Brain Res 44(2):636-640.

Rawley JB, Constantinidis C. 2009. Neural correlates of learning and working memory in the primate posterior parietal cortex. Neurobiol Learn Mem 91(2):129-138.

Reep RL, Chandler HC, King V, Corwin JV. 1994. Rat posterior parietal cortex: topography of corticocortical and thalamic connections. Exp Brain Res 100(1):67-84.

Reep RL, Corwin JV. 1999. Topographic organization of the striatal and thalamic connections of rat medial agranular cortex. Brain Res 841(1-2):43-52.

Reep RL, Corwin JV, Cheatwood JL, Van Vleet TM, Heilman KM, Watson RT. 2004. A rodent model for investigating the neurobiology of contralateral neglect. Cogn Behav Neurol 17(4):191-194.

Robertson RT. 1976. Thalamic projections to visually responsive regions of parietal cortex. Brain Res Bull 1(5):459-469.

Robertson RT. 1977. Thalamic projections to parietal cortex. Brain Behav Evol 14(3):161-184.

Robertson RT, Cunningham TJ. 1981. Organization of corticothalamic projections from parietal cortex in cat. J Comp Neurol 199(4):569-585.

Robertson RT, Rinvik E. 1973. The corticothalamic projections from parietal regions of the cerebral cortex. Experimental degeneration studies in the cat. Brain Res 51:61-79.

Ryszka A, Heger M. 1979. Afferent connections of the laterodorsal thalamic nucleus in the rat. Neurosci Lett 15(1):61-64.

Sanderson KJ, Dreher B, Gayer N. 1991. Prosencephalic connections of striate and extrastriate areas of rat visual cortex. Exp Brain Res 85(2):324-334.

Saporta S, Kruger L. 1977. The organization of thalamocortical relay neurons in the rat ventrobasal complex studied by the retrograde transport of horseradish peroxidase. J Comp Neurol 174(2):187-208.

Save E, Moghaddam M. 1996. Effects of lesions of the associative parietal cortex on the acquisition and use of spatial memory in egocentric and allocentric navigation tasks in the rat. Behav Neurosci 110(1):74-85.

Save E, Poucet B. 2000. Involvement of the hippocampus and associative parietal cortex in the use of proximal and distal landmarks for navigation. Behav Brain Res 109(2):195-206.

Schmahmann JD, Pandya DN. 1990. Anatomical investigation of projections from thalamus to posterior parietal cortex in the rhesus monkey: a WGA-HRP and fluorescent tracer study. J Comp Neurol 295(2):299-326.

Thomas HC, Espinoza SG. 1987. Relationships between interhemispheric cortical connections and visual areas in hooded rats. Brain Res 417(2):214-224.

Toldi J, Feher O, Wolff JR. 1986. Sensory interactive zones in the rat cerebral cortex. Neuroscience 18(2):461-465.

Vertes RP, Linley SB, Groenewegen HJ, Witter MP. 2014. Thalamus. In: Paxinos G, ed. The Rat Nervous System. Fourth edition ed. p 335-390.

Wagor E, Mangini NJ, Pearlman AL. 1980. Retinotopic organization of striate and extrastriate visual cortex in the mouse. J Comp Neurol 193(1):187-202.

Wang Q, Burkhalter A. 2007. Area map of mouse visual cortex. J Comp Neurol 502(3):339-357.

Wang Q, Gao E, Burkhalter A. 2011. Gateways of ventral and dorsal streams in mouse visual cortex. J Neurosci 31(5):1905-1918.

Welker C. 1971. Microelectrode delineation of fine grain somatotopic organization of (SmI) cerebral neocortex in albino rat. Brain Res 26(2):259-275.

Whitlock JR, Pfuhl G, Dagslott N, Moser MB, Moser EI. 2012. Functional split between parietal and entorhinal cortices in the rat. Neuron 73(4):789-802.

Whitlock JR, Sutherland RJ, Witter MP, Moser MB, Moser EI. 2008. Navigating from hippocampus to parietal cortex. Proc Natl Acad Sci U S A 105(39):14755-14762.

Wilber A, Clark BJ, Demecha AJ, Mesina L, Vos JM, McNaughton BL. 2015. Cortical Connectivity Maps Reveal Anatomically Distinct Areas in the Parietal Cortex of the Rat. Frontiers in Neural Circuits 8.

Wilber AA, Clark BJ, Forster TC, Tatsuno M, McNaughton BL. 2014. Interaction of egocentric and world-centered reference frames in the rat posterior parietal cortex. J Neurosci 34(16):5431-5446.

Wise SP, Jones EG. 1977. Cells of origin and terminal distribution of descending projections of the rat somatic sensory cortex. J Comp Neurol 175(2):129-157.

Yeterian EH, Pandya DN. 1985. Corticothalamic connections of the posterior parietal cortex in the rhesus monkey. J Comp Neurol 237(3):408-426.

Zahm DS, Parsley KP, Schwartz ZM, Cheng AY. 2013. On lateral septum-like characteristics of outputs from the accumbal hedonic "hotspot" of Pecina and Berridge with commentary on the transitional nature of basal forebrain "boundaries". J Comp Neurol 521(1):50-68.

**Resources cited**

Adobe Photoshop CS6: Adobe Systems Incorporated, San Jose, http://www.adobe.com/no/products/cs6.html; RRID: SCR_014199

Adobe Illustrator CS6: Adobe Systems Incorporated, http://www.adobe.com/no/products/cs6.html; RRID: SCR_014198

Neurolucida: MicroBrightField, Colchester, VT, http://www.mbfbioscience.com/neurolucida; RRID: SCR_001775

ImageJ: http://rsb.info.nih.gov/ij/index.html; RRID: SCR_003070

| Antibody | Immunogen | Source | Dilution |
|---|---|---|---|
| Anti-parvalbumin | Frog muscle parvalbumin | Sigma-Aldrich #P3088, RRID: AB_477329, mouse monoclonal IgG1 antibody, clone PARV-19 | 1:1,000 |
| Anti-type 2 muscarinic acetylcholine receptor | i3 loop of m2 receptor fusion protein (225-359), fused to Glutathione S-transferase | Merck Millipore #MAB367, RRID: AB_94952, rat monoclonal IgG2a antibody, clone M2-2-B3 | 1:750 |
| Anti-*Phaseolus vulgaris* Leucoagglutinin | *Phaseolus vulgaris* Leucoagglutinin (E + L) | Vector Laboratories #AS-2224, RRID: AB_10000080, goat polyclonal antibody | 1:1,000 |

**Table 1:** List of primary antibodies used in this study.

| | |
|---|---|
| **Cortical areas** | |
| PPC | Posterior parietal cortex |
| mPPC | Medial posterior parietal cortex |
| lPPC | Lateral posterior parietal cortex |
| PtP | Posterior part of parietal cortex |
| M | Motor cortex |
| M1 | Primary motor cortex |
| M2 | Secondary motor cortex |
| S1 | Primary somatosensory cortex |
| S2 | Secondary somatosensory cortex |
| V1 | Primary visual cortex |
| V2L | Lateral secondary visual cortex |
| V2M | Medial secondary visual cortex |
| AuD | Auditory cortex |
| RSC | Retrosplenial cortex |
| **Visualized protein** | |
| M2AChR | Muscarinic acetylcholine receptor type 2 |
| **Directional arrows** | |
| C | Caudal |
| L | Lateral |
| M | Medial |
| R | Rostral |
| **Tracers used** | |
| B/BDA | Biotinylated dextran amine, 10 kDa |
| DY | Diamidino yellow |
| FB | Fast Blue |
| FG | Fluorogold |
| P/PHA-L | *Phaseolus Vulgaris* Leucoagglutinin |
| **Thalamic nuclei** | |
| AD | Anterodorsal nucleus |
| AM | Anteromedial nucleus |
| Ang | Angular nucleus |
| AP | Anterior pretectal nucleus |
| AV | Anteroventral nucleus |
| CL | Centrolateral nucleus |
| CM | Central medial nucleus |
| DLG | Dorsal lateral geniculate nucleus |
| LD | Laterodorsal nucleus |
| LDl | Laterodorsal nucleus, lateral part |
| LDm | Laterodorsal nucleus, medial part |
| LP | Lateral posterior nucleus |
| LPl | Lateral posterior nucleus, lateral part |
| LPmc | Lateral posterior nucleus, caudomedial part |
| LPmr | Lateral posterior nucleus, rostromedial part |
| MD | Mediodorsal nucleus |
| MG | Medial geniculate nucleus |
| OPC | Oval paracentral nucleus |
| PAG | Periaqueductal gray |
| PC | Paracentral nucleus |
| PF | Parafascicular nucleus |
| Po | Posterior thalamic nuclear group |
| PT | Paratenial nucleus |
| PV | Paraventricular nucleus |
| Re | Reuniens nucleus |
| Rh | Rhomboid nucleus |
| Rt | Reticular nucleus |
| SPFPC | Subparafascicular nucleus, parvicellular part |
| Sub | Submedius nucleus |
| VA | Ventral anterior nucleus |
| VL | Ventrolateral nucleus |
| VLG | Ventral lateral geniculate nucleus |
| VM | Ventromedial nucleus |
| VP | Ventral posterior nucleus |
| VPl | Ventral posterior nucleus, lateral part |
| VPm | Ventral posterior nucleus, medial part |
| VPPC | Ventral posterior nucleus, parvicellular part |
| ZI | Zona incerta |

**Table 2:** List of abbreviations

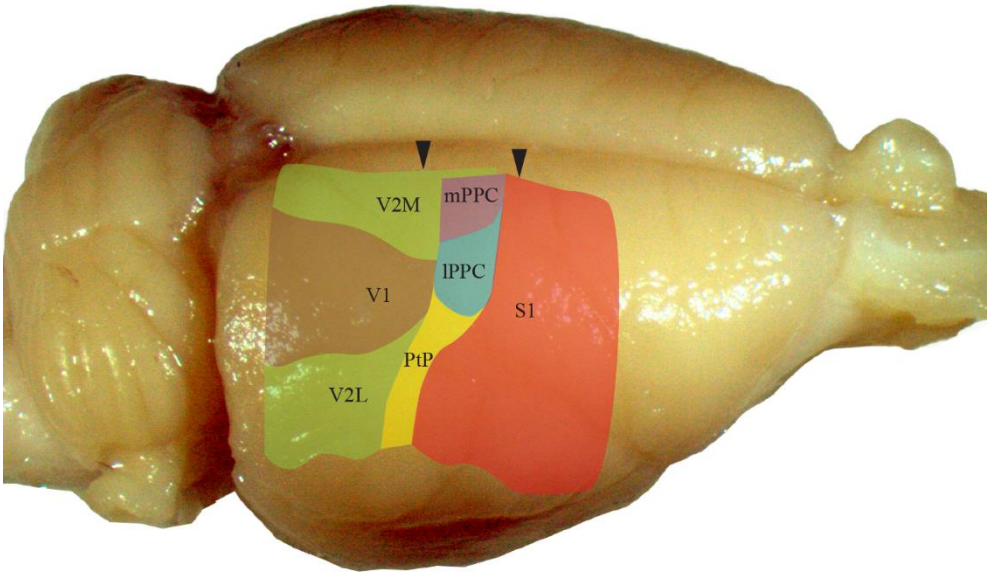


**Figure 1**. Schematic of the topography of the caudal cortex in rat based on the Rat Brain Atlas (Paxinos and Watson, 2007). Indicated with arrowheads is the approximate location of the most rostral and most caudal coronal section in Figure 2. Outlines of cortical areas have been colorcoded: primary somatosensory cortex in red; medial posterior parietal cortex in purple; lateral posterior parietal cortex in blue; parietal cortex, posterior area in yellow; primary visual cortex in brown; secondary visual cortices in green. See Table 2 for list of abbreviations.

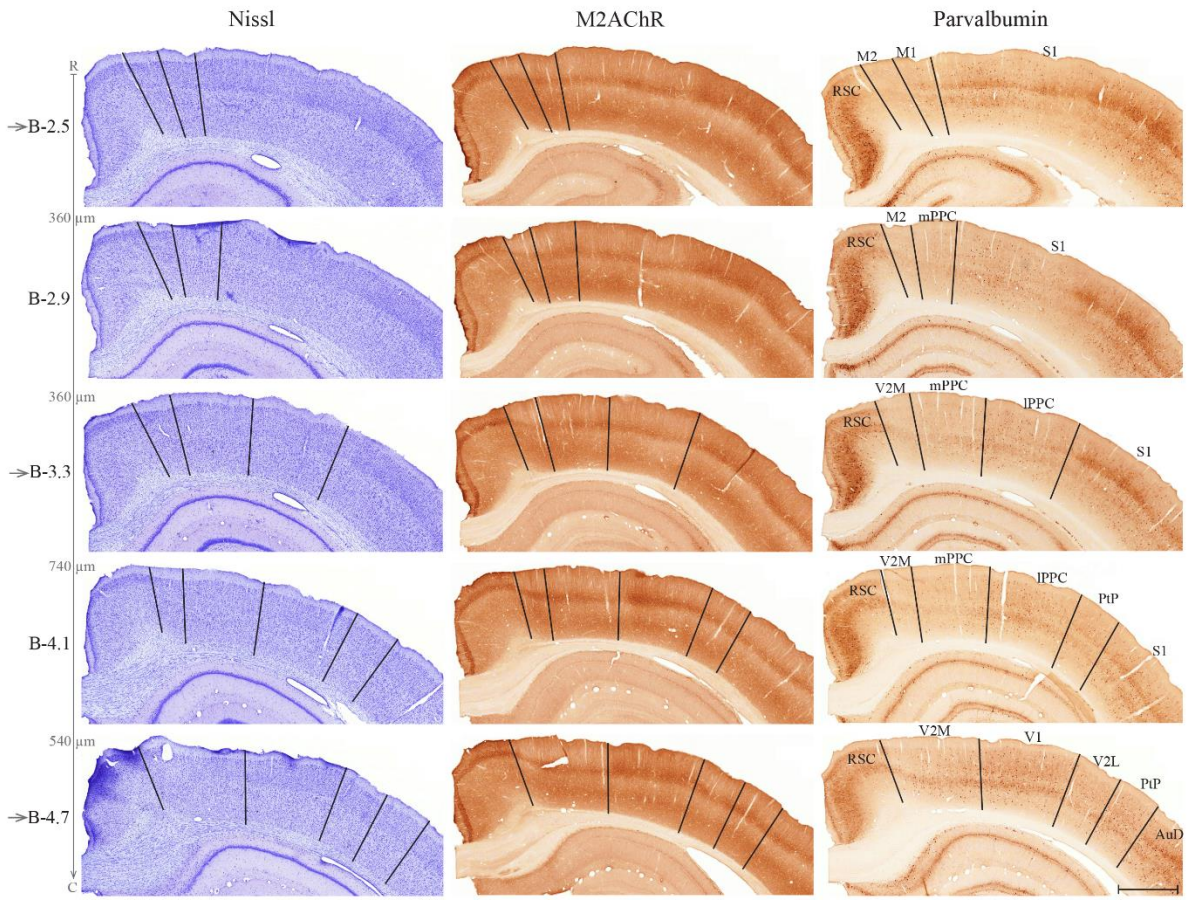


**Figure 2**. Delineation of cortical areas in coronal sections based on cytoarchitecture (Nissl stain, left column) as well as the distribution of the type 2 muscarinic acetylcholine receptor, (M2AChR, middle column) and parvalbumin (right column). On the left side, indicated in black numbers, is the distance of the section from bregma according to Paxinos and Watson (2007). Gray numbers on the rostrocaudal axis correspond to the actual distance between sections, based on 30 µm sections. The distances decided by the two methods may differ slightly, for instance the total distance between the most rostral and the most caudal section according to the atlas is 2.2 mm whereas the measured distance is 1.98 mm. The difference may arise from a variation in brain size, or the designation of bregma-level by comparison with the atlas may be slightly off due to a difference in the cutting angle of the brains. Horizontal black arrows indicate the approximate coronal level of dashed lines shown in Figure 3. Scalebar 1 mm. Nomenclature is mainly adopted from Paxinos and Watson (2007). See Table 2 for list of abbreviations.

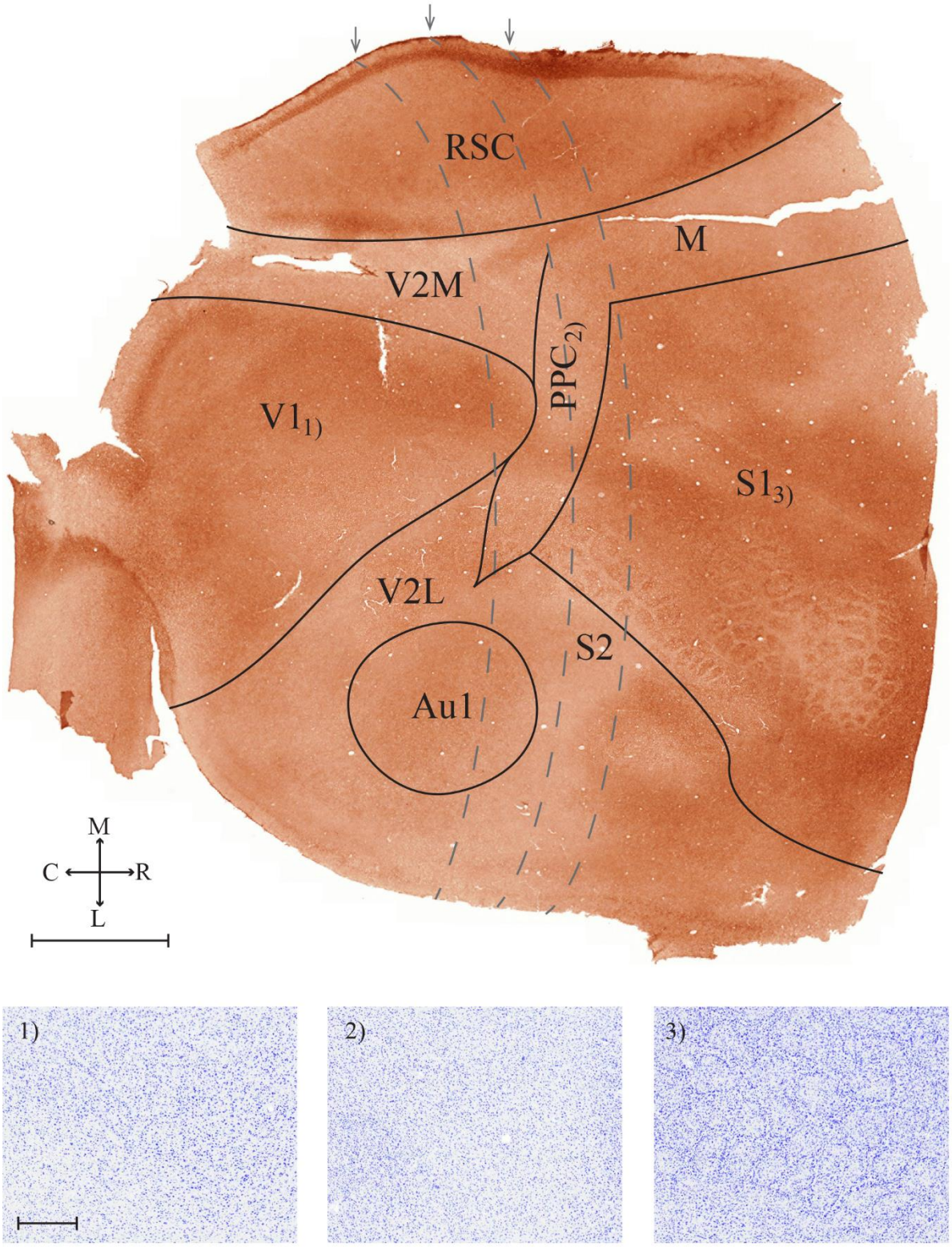


**Figure 3**. Delineation of cortical areas in a flat section through layer 4 of the dorsal caudal cortex stained for the type 2 muscarinic acetylcholine receptor. When a curved structure such as the cortex of a rat brain is flattened, lines that were originally straight in the intact structure

will be distorted and rounded in the flattened structure. The dashed lines correspond to three of the coronal sections illustrated in Figure 2 marked with arrowheads. The lines are rounded and approximately parallel to the rostral edge of the section, since this line was cut straight in the intact brain. Scalebar 2 mm. Insets: 1) primary visual cortex, 2) posterior parietal cortex, and 3) the barrel region of primary somatosensory cortex in corresponding Nissl-stained sections. Inset scalebar 500 µm. See Table 2 for list of abbreviations.

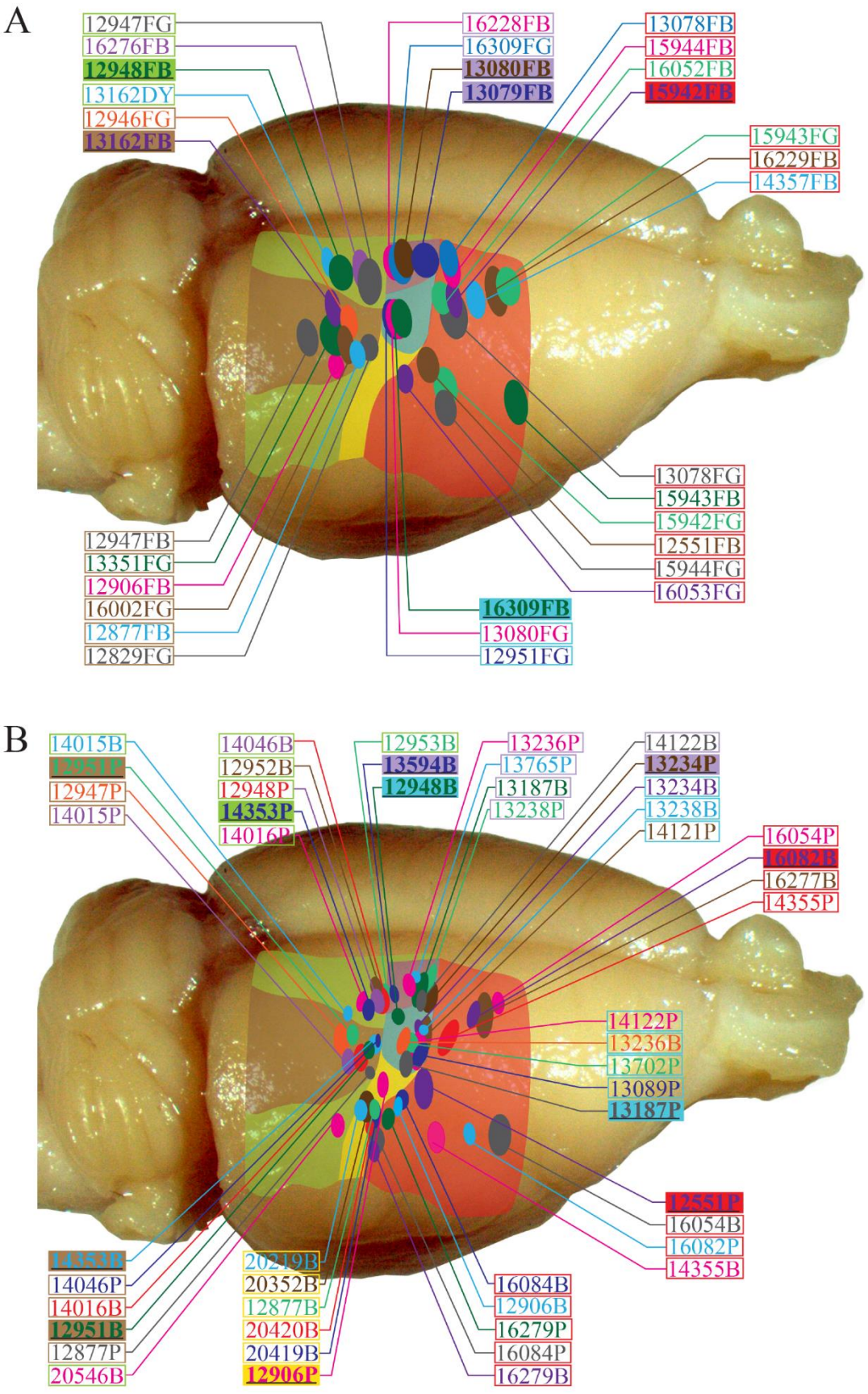
A
12947FG
16276FB
12948FB
13162DY
12946FG
13162FB
16228FB
16309FG
13080FB
13079FB
13078FB
15944FB
16052FB
15942FB
15943FG
16229FB
14357FB
13078FG
15943FB
15942FG
12551FB
15944FG
16053FG
12947FB
13351FG
12906FB
16002FG
12877FB
12829FG
16309FB
13080FG
12951FG
B
14015B
12951P
12947P
14015P
14046B
12952B
12948P
14353P
14016P
12953B
13594B
12948B
13236P
13765P
13187B
13238P
14122B
13234P
13234B
13238B
14121P
16054P
16082B
16277B
14355P
14122P
13236B
13702P
13089P
13187P
12551P
16054B
16082P
14355B
14353B
14046P
14016B
12951B
12877P
20546B
20219B
20352B
12877B
20420B
20419B
12906P
16084B
12906B
16279P
16084P
16279B

**Figure 4**. Representation of the cores of injections of retrograde (a) and anterograde (b) tracers, positioned on a picture of a rat brain. Cortical areas are delineated according to own established criteria, coinciding with those of Paxinos and Watson (2007) and colorcoded as in Figure 1. The color of the text boxes corresponds to which area was injected, the color of the text corresponds to the color of the respective injection representation in the figure. Numbers correspond to the animal's number which was assigned upon arrival to the facility, and letters indicate which tracer was injected. Injections with illustrated thalamic labeling patterns are highlighted. See Table 2 for list of abbreviations.

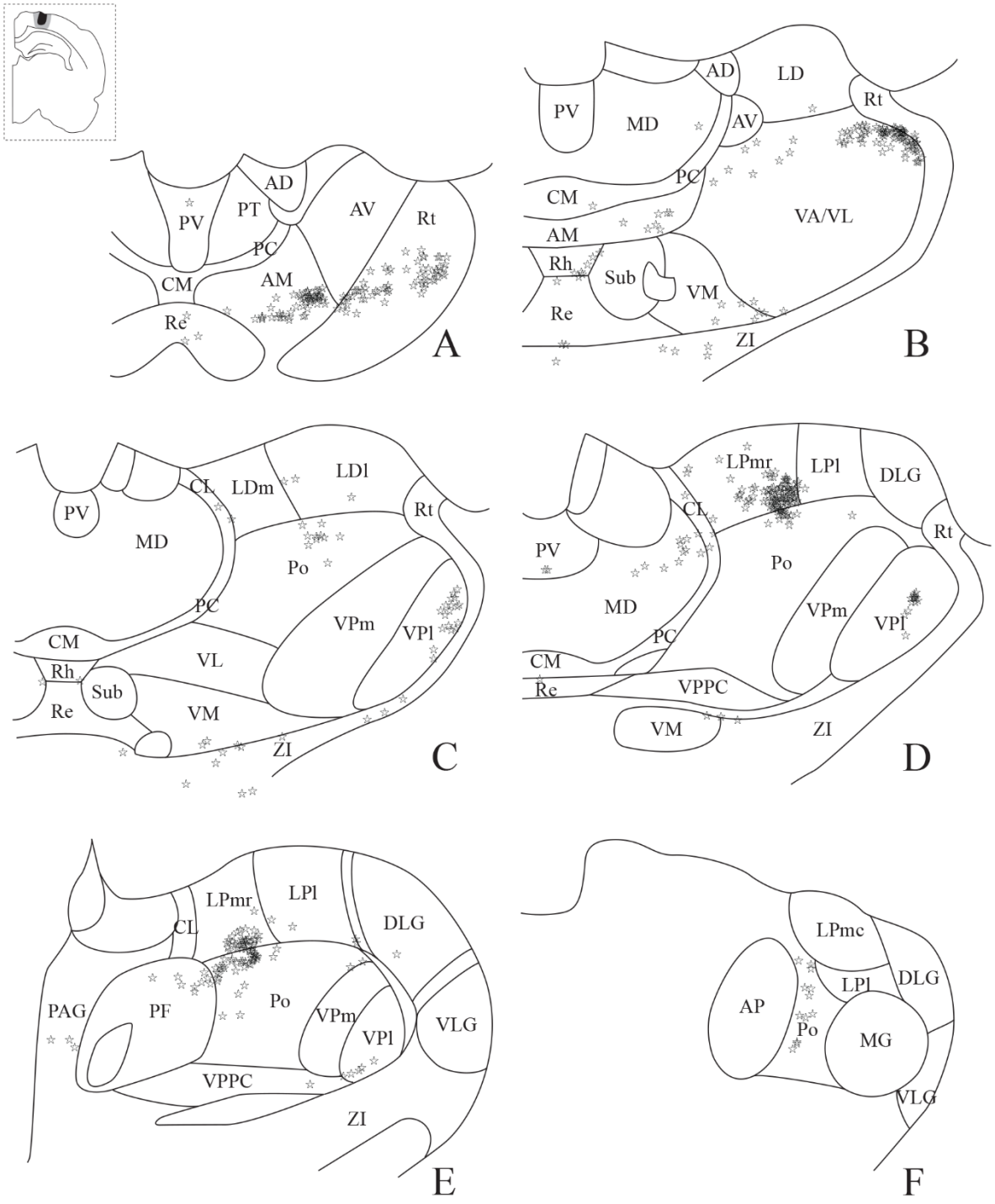


**Figure 5**. Retrogradely labeled cells after injection of Fast Blue rostrally in mPPC. A dense patch of labeled cells was found in LPmr as well as AM. Inset: Drawing of the injection site in a coronal section. See Table 2 for list of abbreviations.

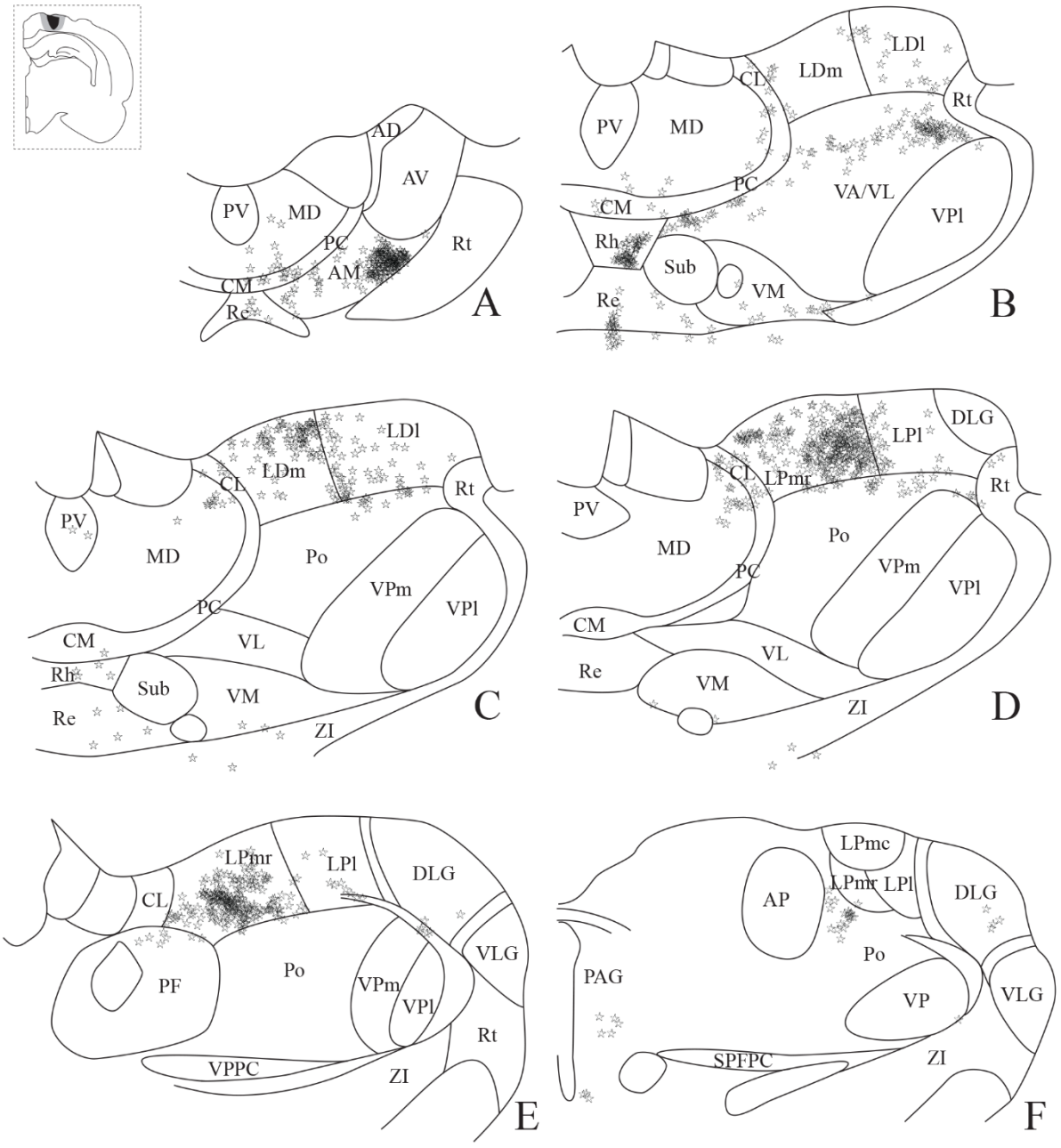


**Figure 6**. Retrogradely labeled cells after injection of Fast Blue caudally in mPPC. A high concentration of labeled cells was seen in LPmr, as well as AM and LDm. Inset: Drawing of the injection site in a coronal section. See Table 2 for list of abbreviations.

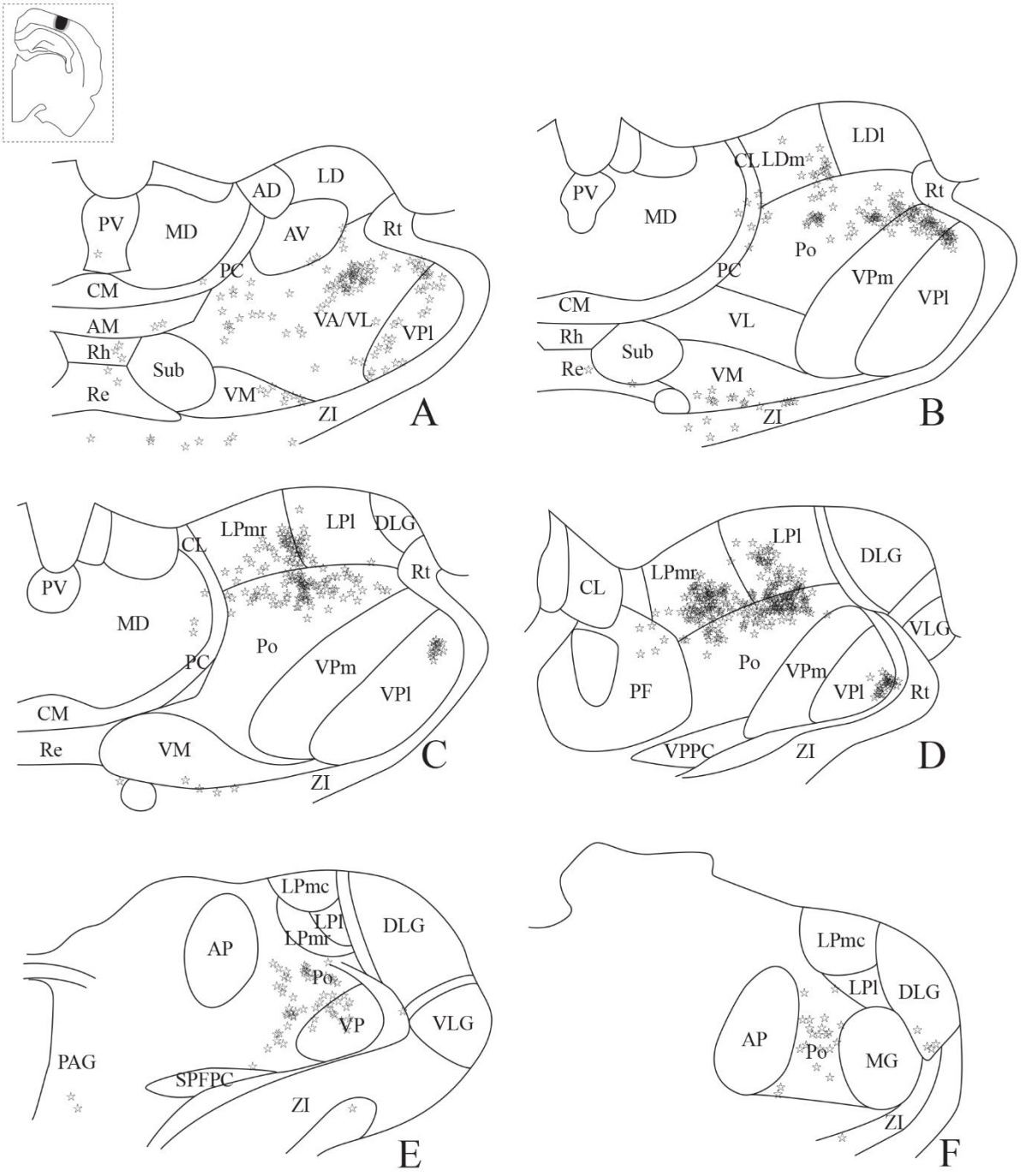


**Figure 7**. Retrogradely labeled cells after injection of Fast Blue in lPPC. Labeled cells were distributed mainly in Po, LPmr and LPl. Inset: Drawing of the injection site in a coronal section. See Table 2 for list of abbreviations.

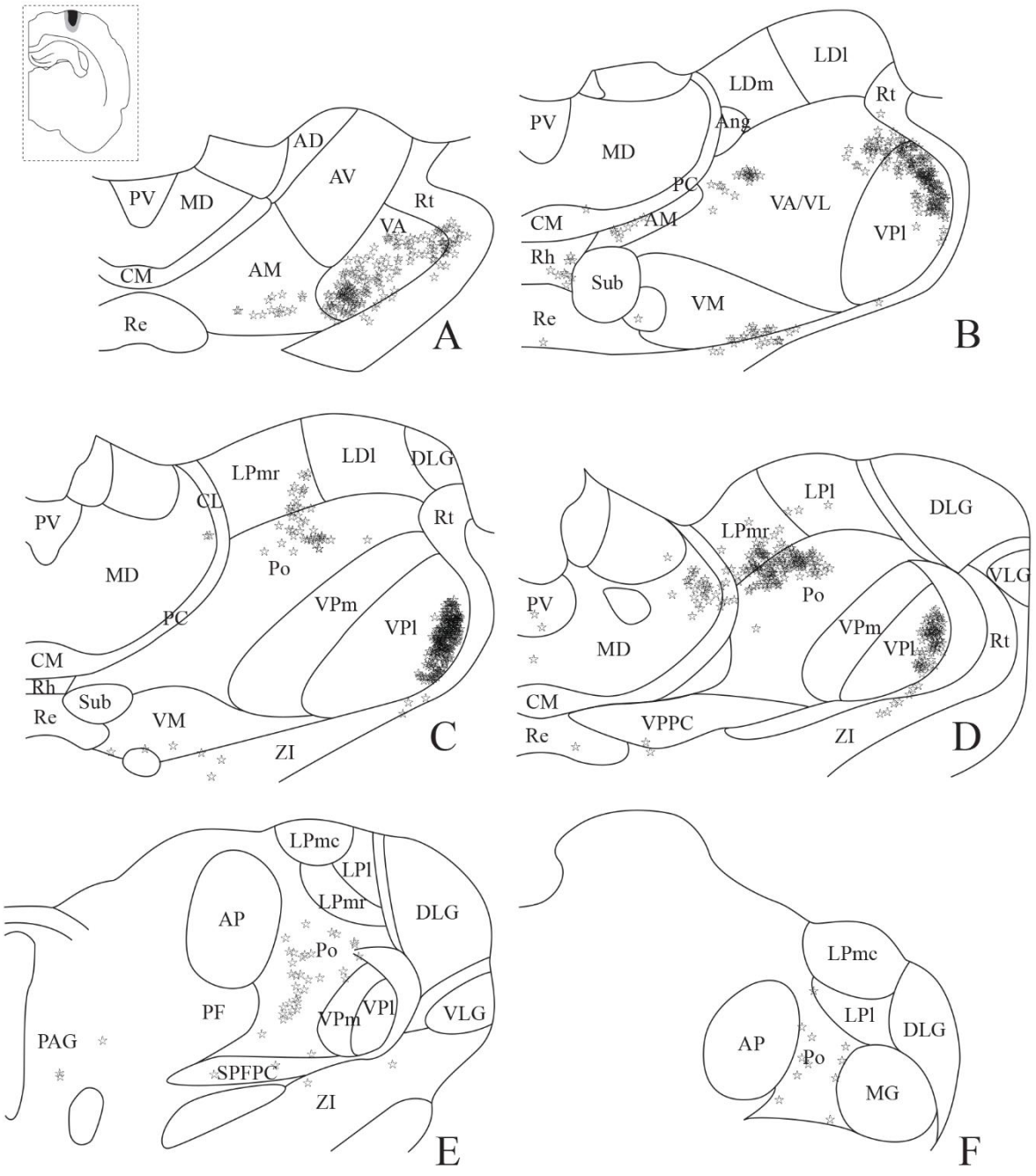


**Figure 8**. Retrogradely labeled cells after injection of Fast Blue in the trunk region of S1. Dense patches of labeled cells were observed in VPl and Po. Inset: Drawing of the injection site in a coronal section. See Table 2 for list of abbreviations.

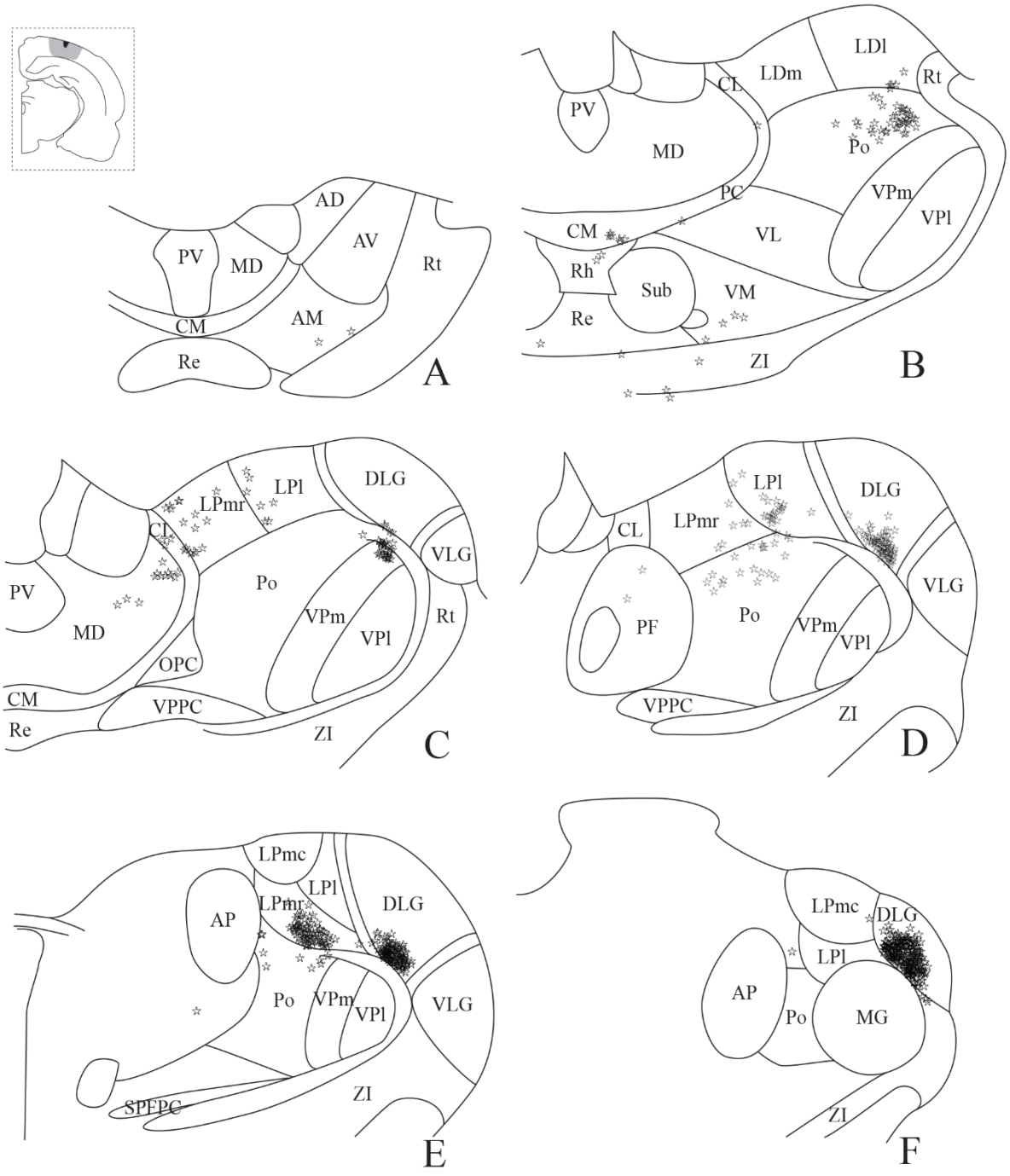


**Figure 9**. Retrogradely labeled cells after injection of Fast Blue in V1. Labeled cells were found in high concentration in DLG as well as caudal LPmr. Inset: Drawing of the injection site in a coronal section. See Table 2 for list of abbreviations.

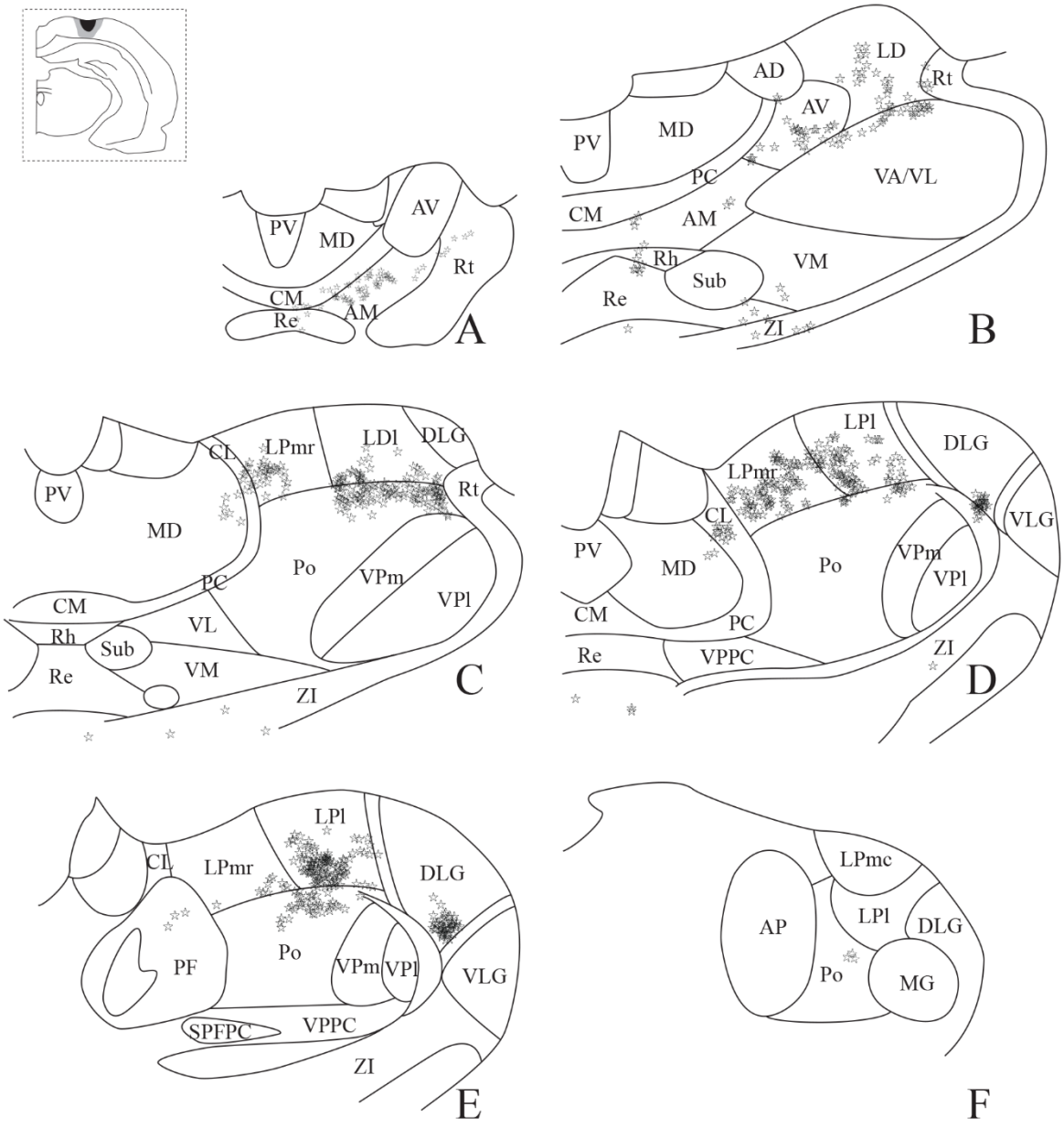


**Figure 10**. Retrogradely labeled cells after injection of Fast Blue in V2M. Labeled cells were mainly distributed throughout LD and LP nuclei. Inset: Drawing of the injection site in a coronal section. See Table 2 for list of abbreviations.

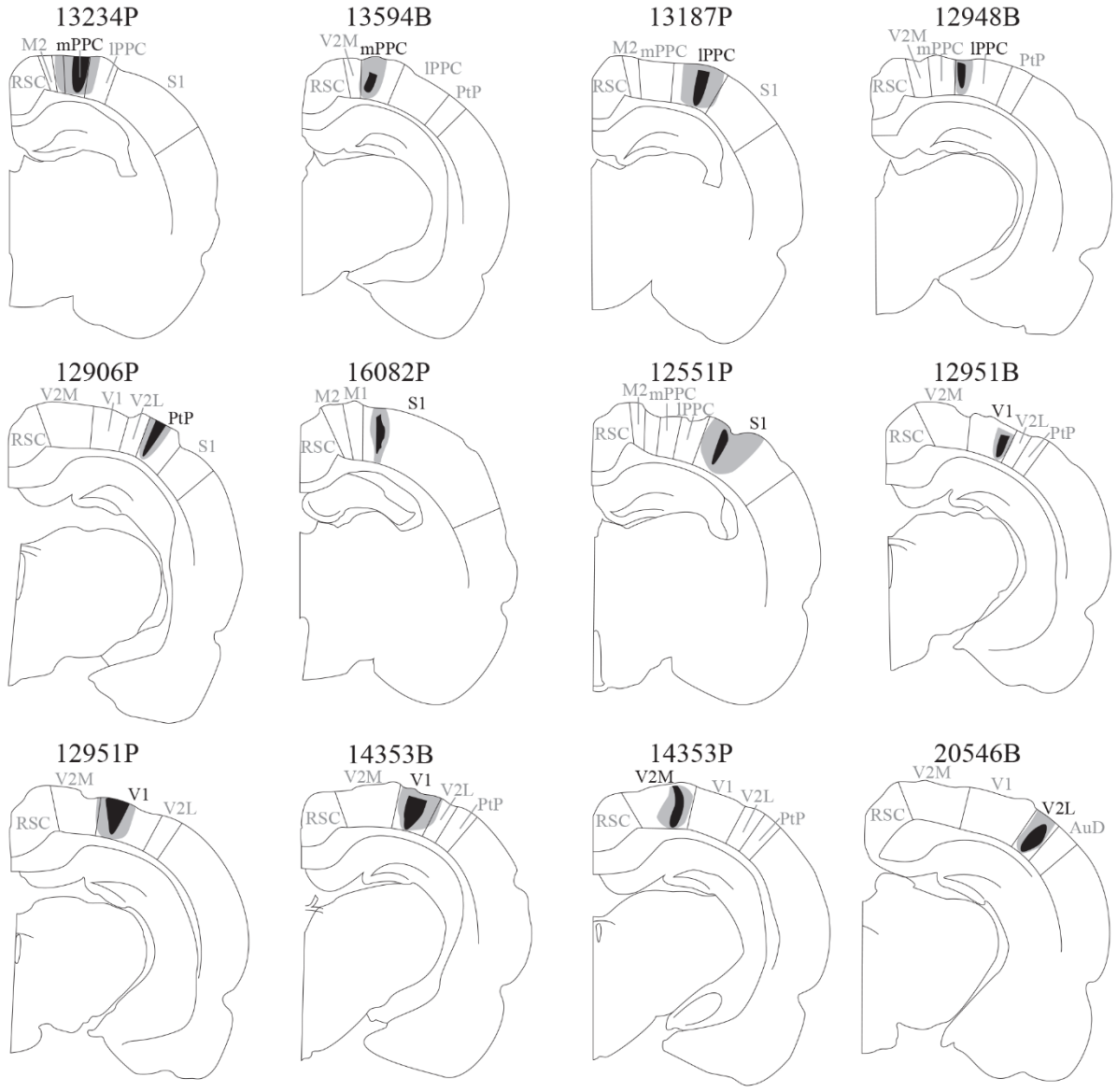


**Figure 11**. Overview of illustrated anterograde tracer injections in coronal sections. Numbers correspond to the number the animal was assigned upon arrival at the animal facility, letters indicate which tracer was injected. See Table 2 for list of abbreviations.

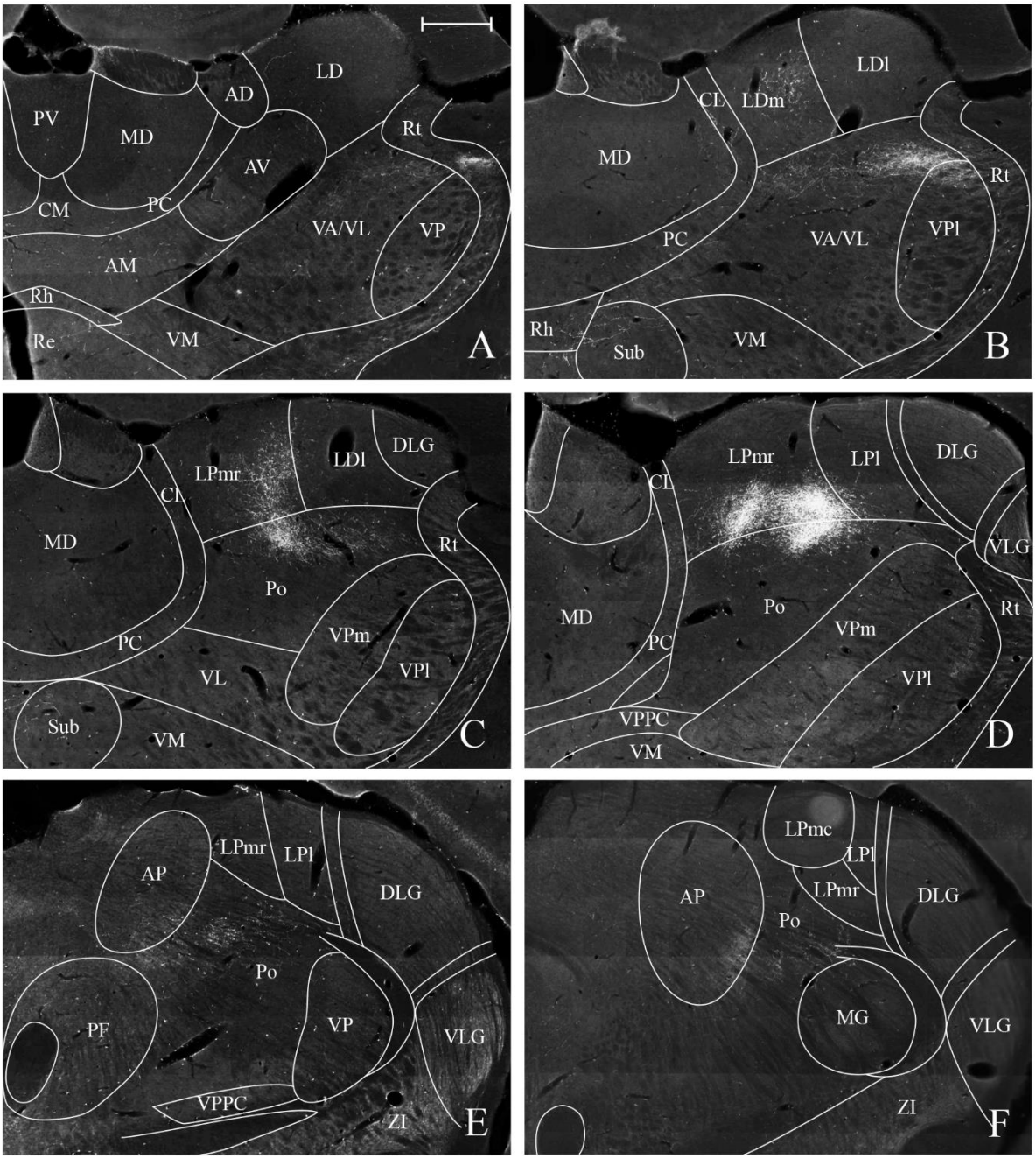


**Figure 12**. Anterogradely labeled fibers after injection of PHA-L rostrally in mPPC. Dense labeling was observed ventrally in LPmr. Scalebar 500 µm. See Table 2 for list of abbreviations.

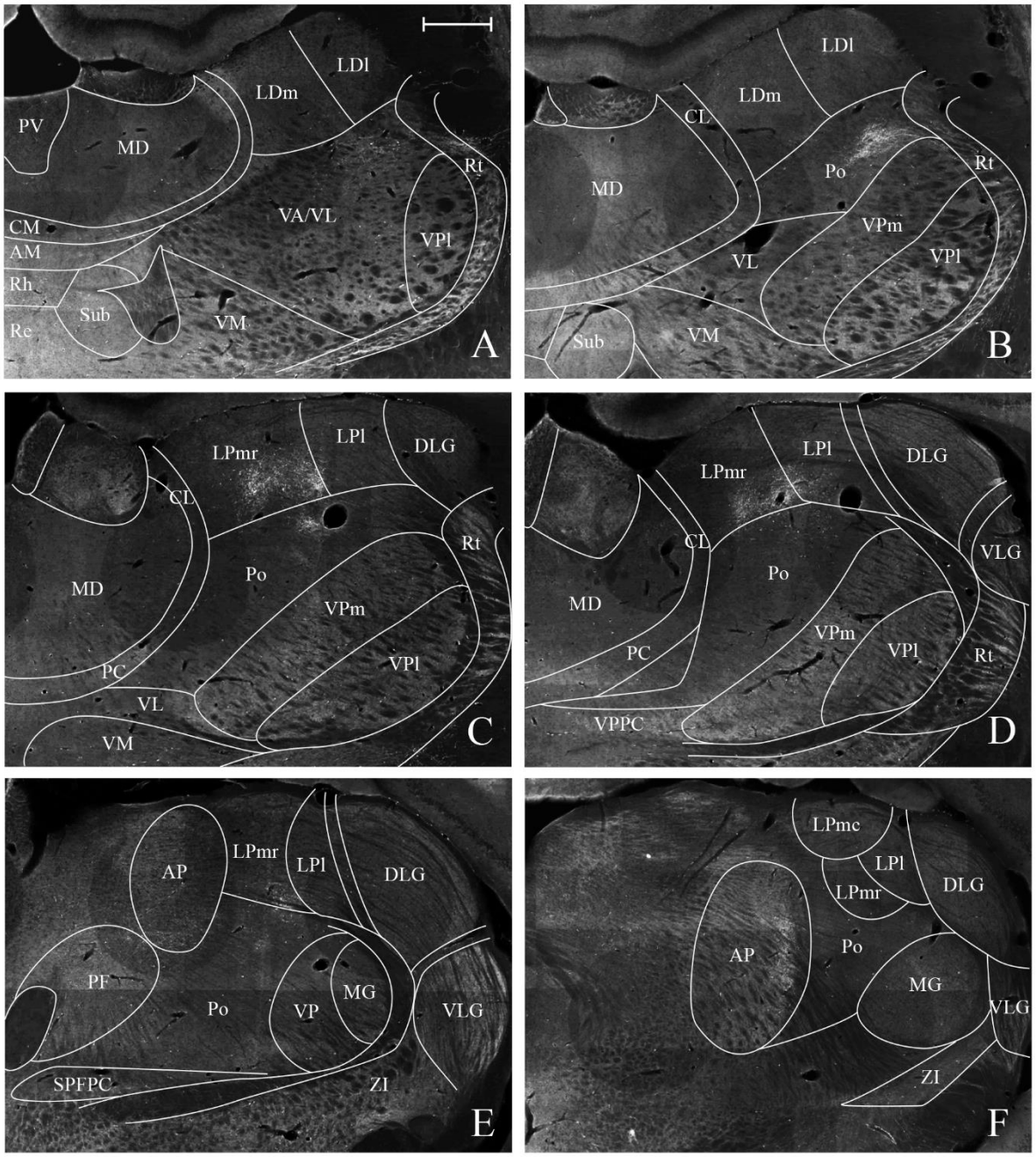


**Figure 13**. Anterogradely labeled fibers after injection of BDA caudally in mPPC. A cluster of labeled fibers was found ventrally in LPmr. Scalebar 500 µm. See Table 2 for list of abbreviations.

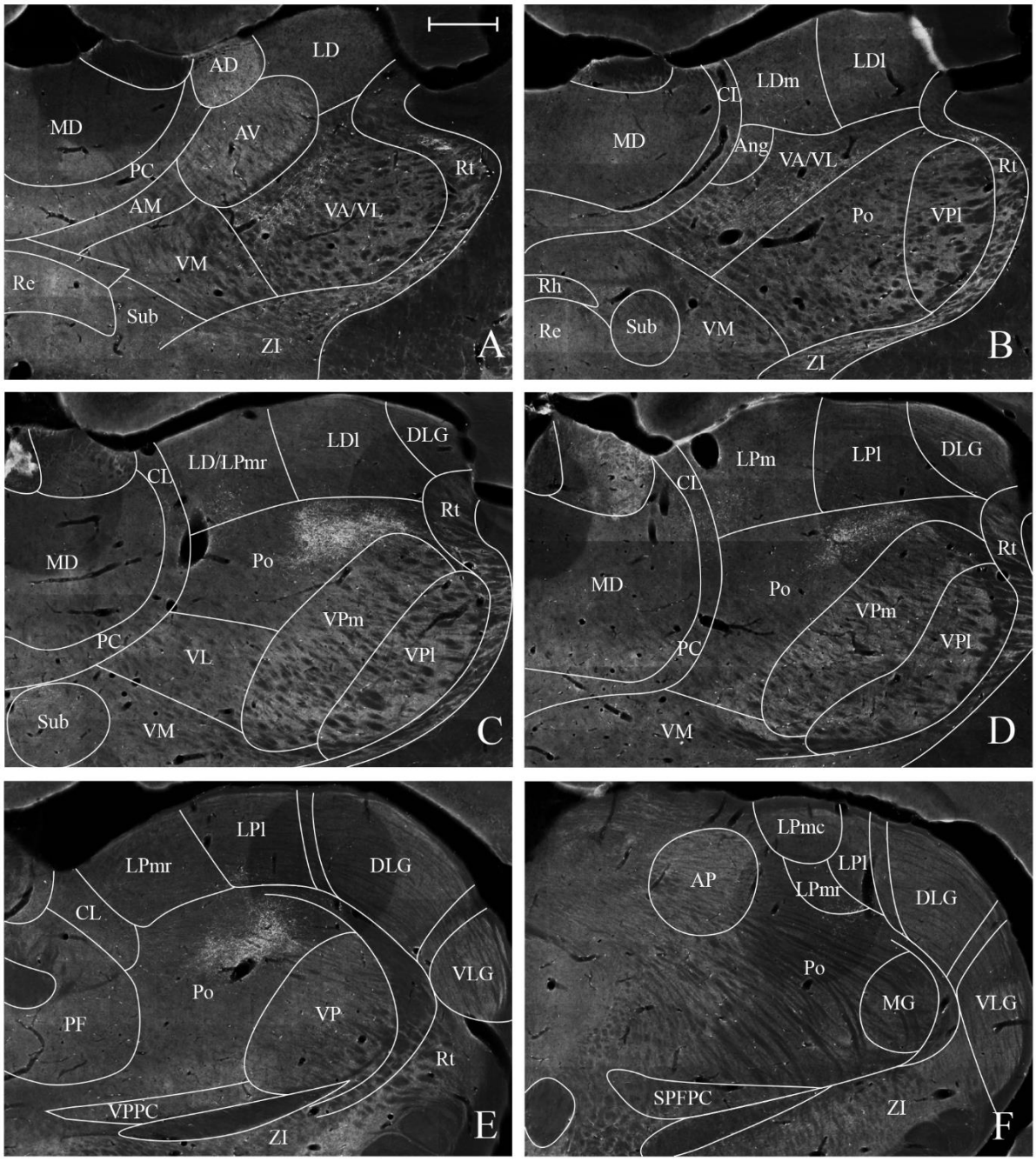


**Figure 14**. Anterogradely labeled fibers after injection of PHA-L rostrally in lPPC. A high concentration of labeled fibers was seen in Po. Scalebar 500 µm. See Table 2 for list of abbreviations.

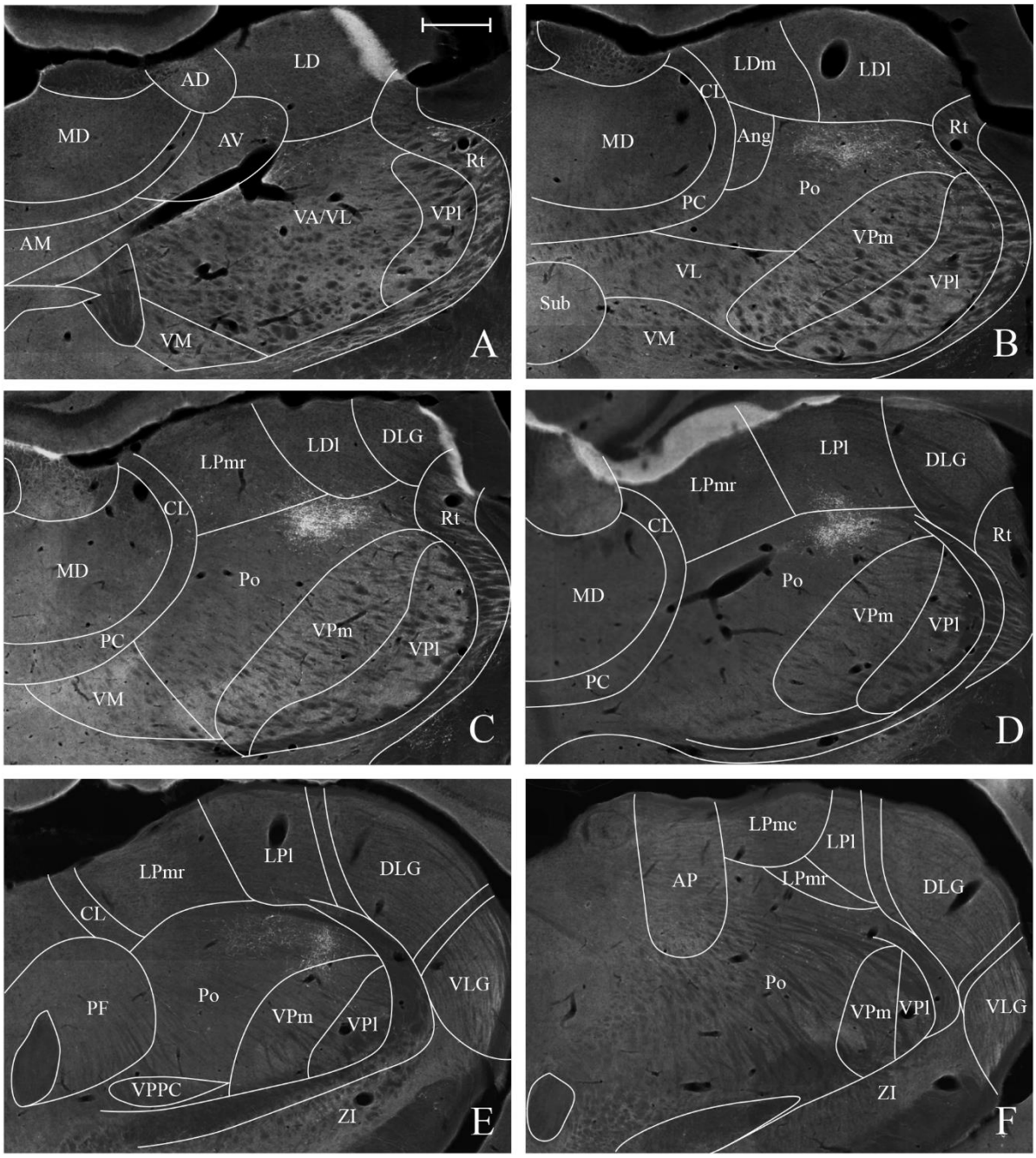


**Figure 15**. Anterogradely labeled fibers after injection of BDA caudally in lPPC. Labeled fibers were clustered in Po. Scalebar 500 µm. See Table 2 for list of abbreviations.

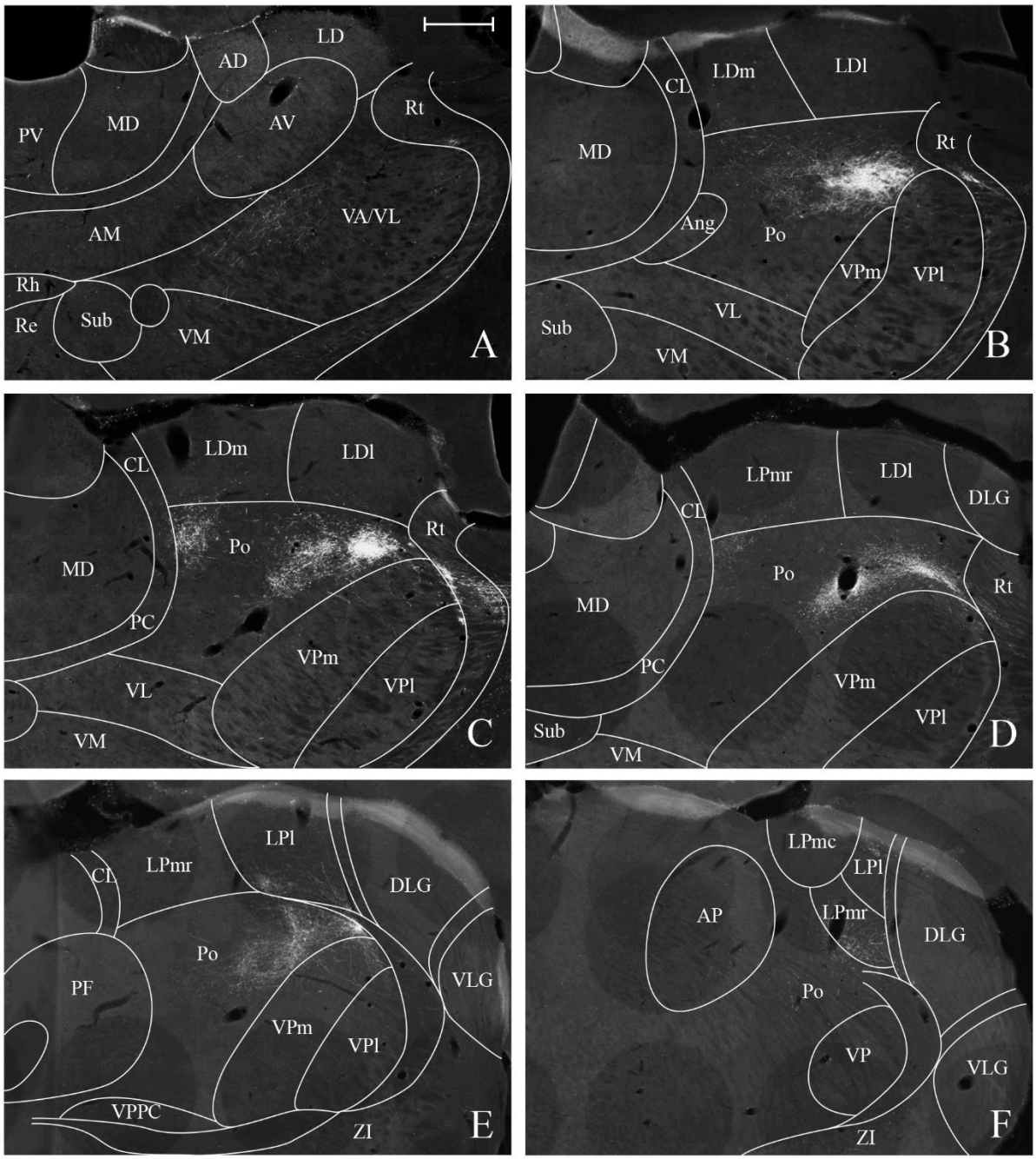


**Figure 16**. Anterogradely labeled fibers after injection of PHA-L in PtP. Dense labeling was found in Po. Scalebar 500 µm. See Table 2 for list of abbreviations.

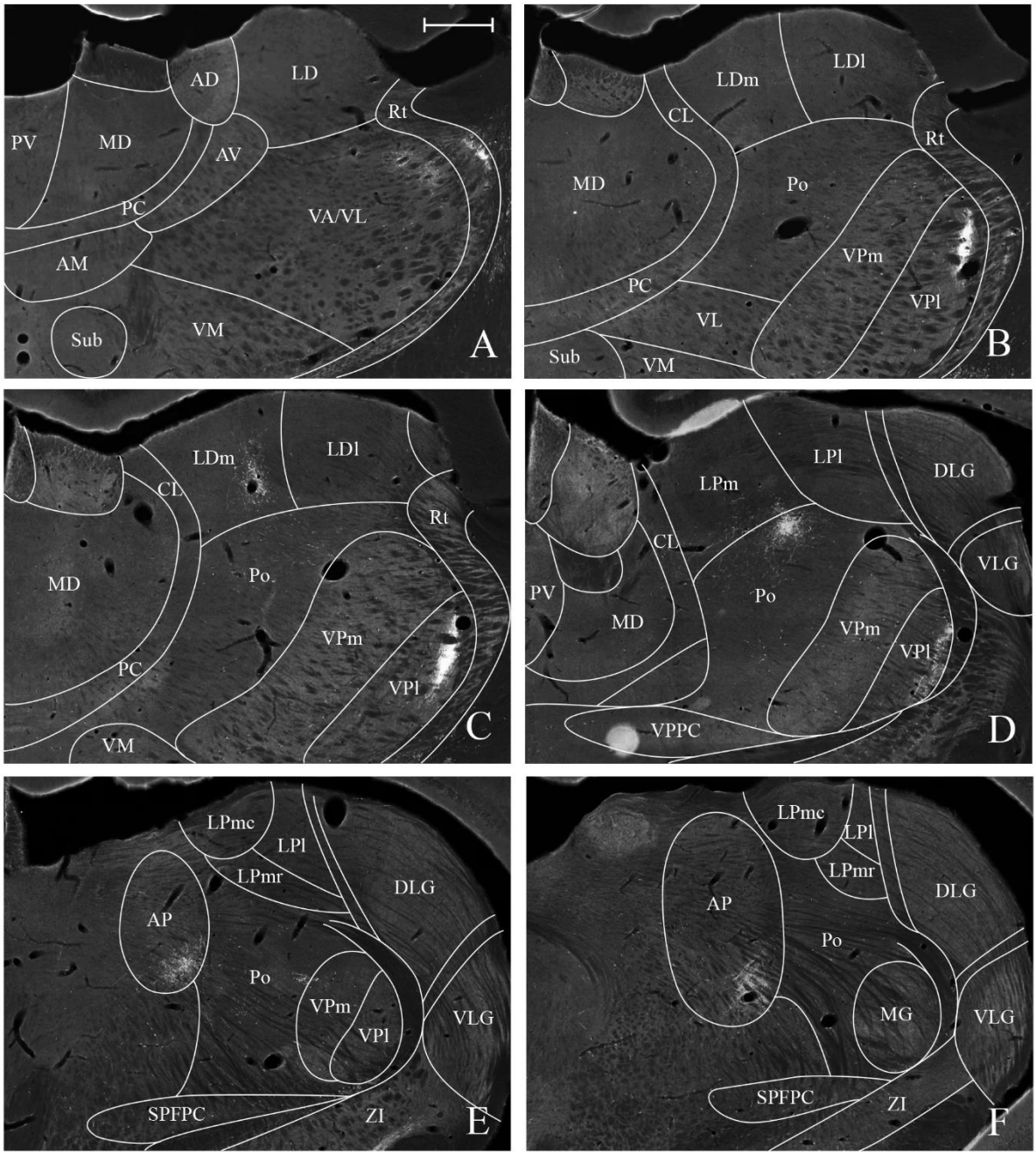


**Figure 17**. Anterogradely labeled fibers after injection of BDA in the hindlimb region of S1. Labeling was densely clustered in VPl and Po. Scalebar 500 µm. See Table 2 for list of abbreviations.

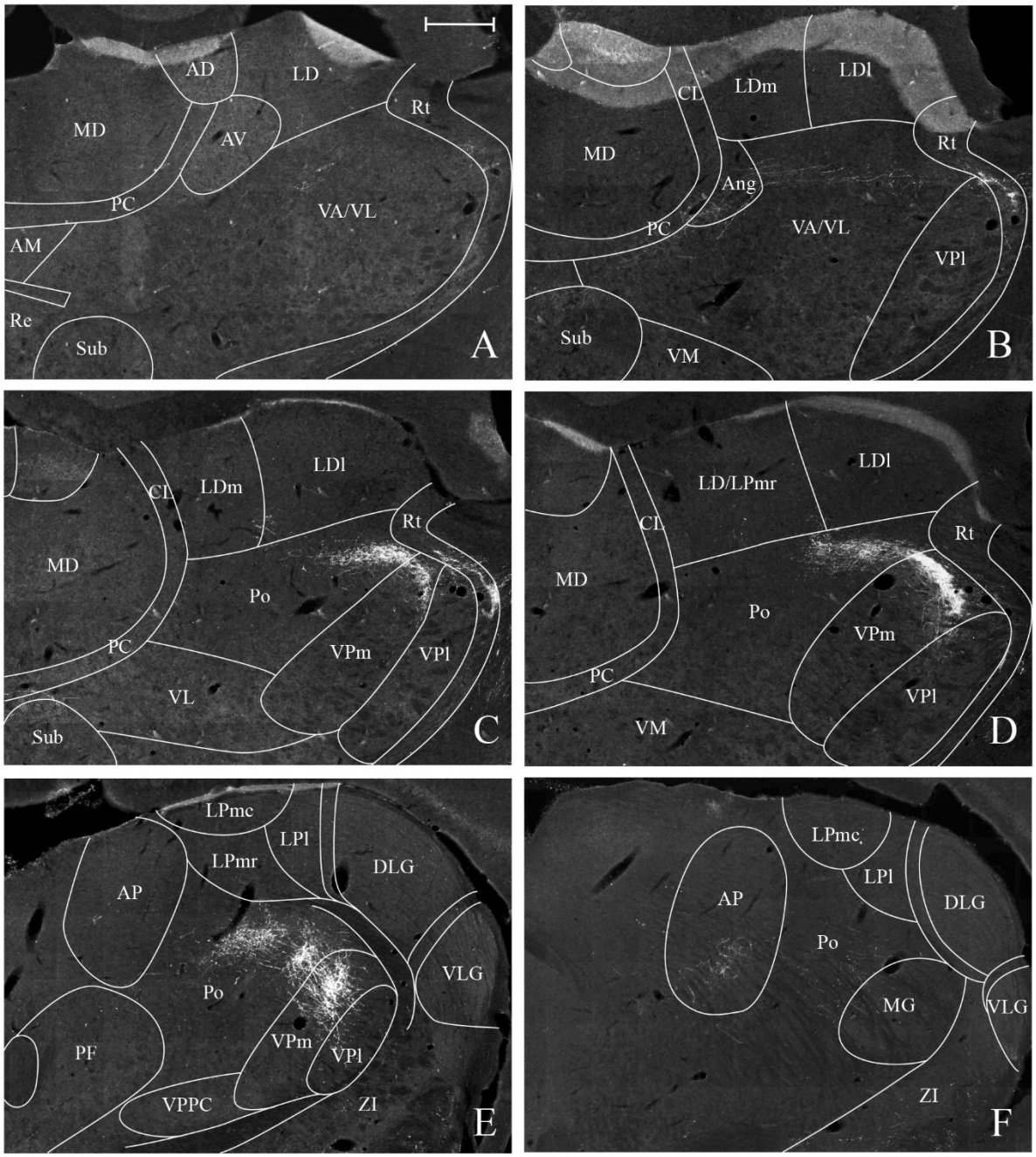


**Figure 18**. Anterogradely labeled fibers after injection of PHA-L in the barrel region of S1. A high concentration of labeled fibers was found in VPm and Po. Scalebar 500 µm. See Table 2 for list of abbreviations.

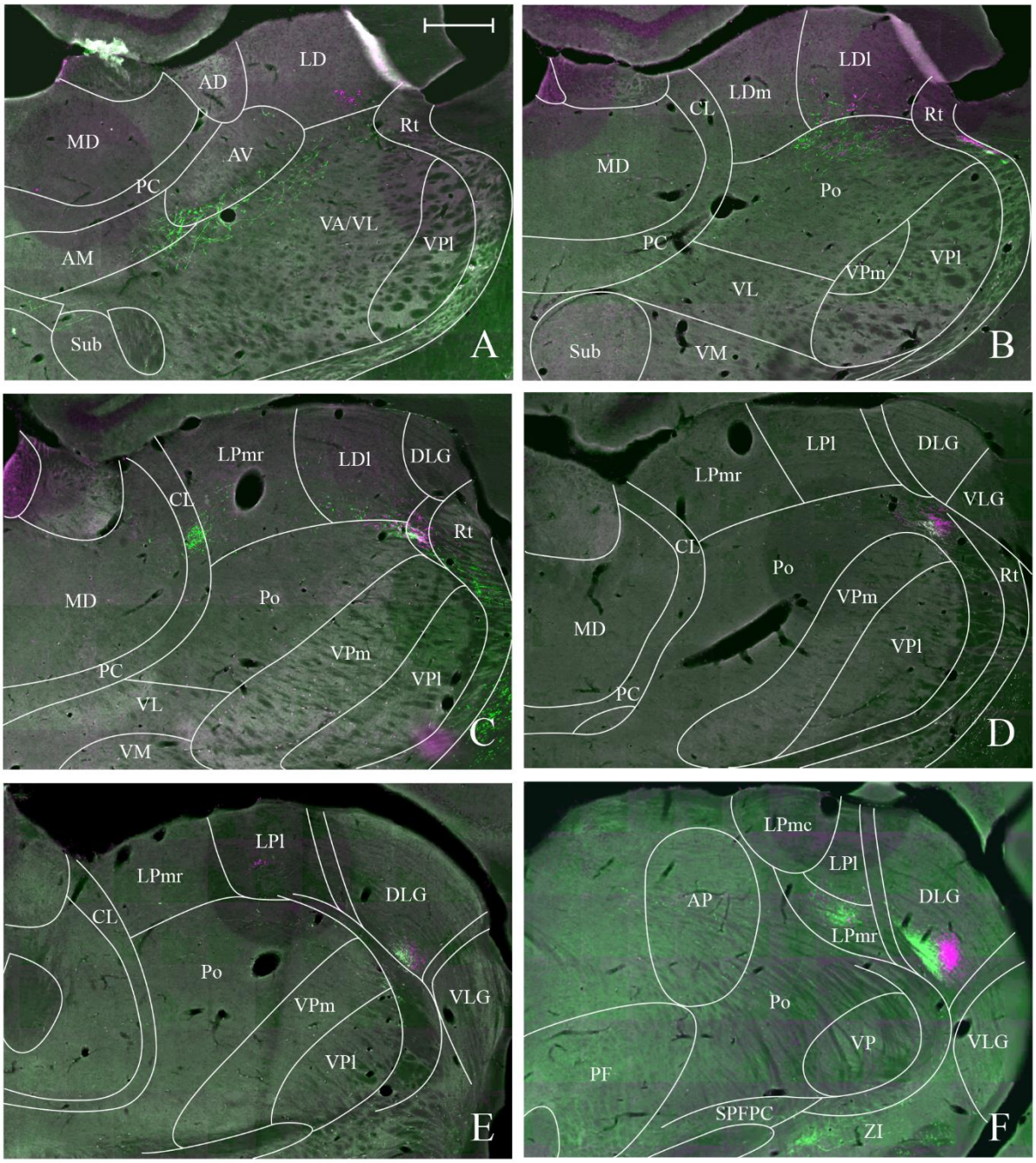


**Figure 19**. Anterogradely labeled fibers after injections of BDA and PHA-L (visualized in green and magenta, respectively) in V1. Both injections resulted in a high density of labeled fibers in DLG. Scalebar 500 µm. See Table 2 for list of abbreviations.

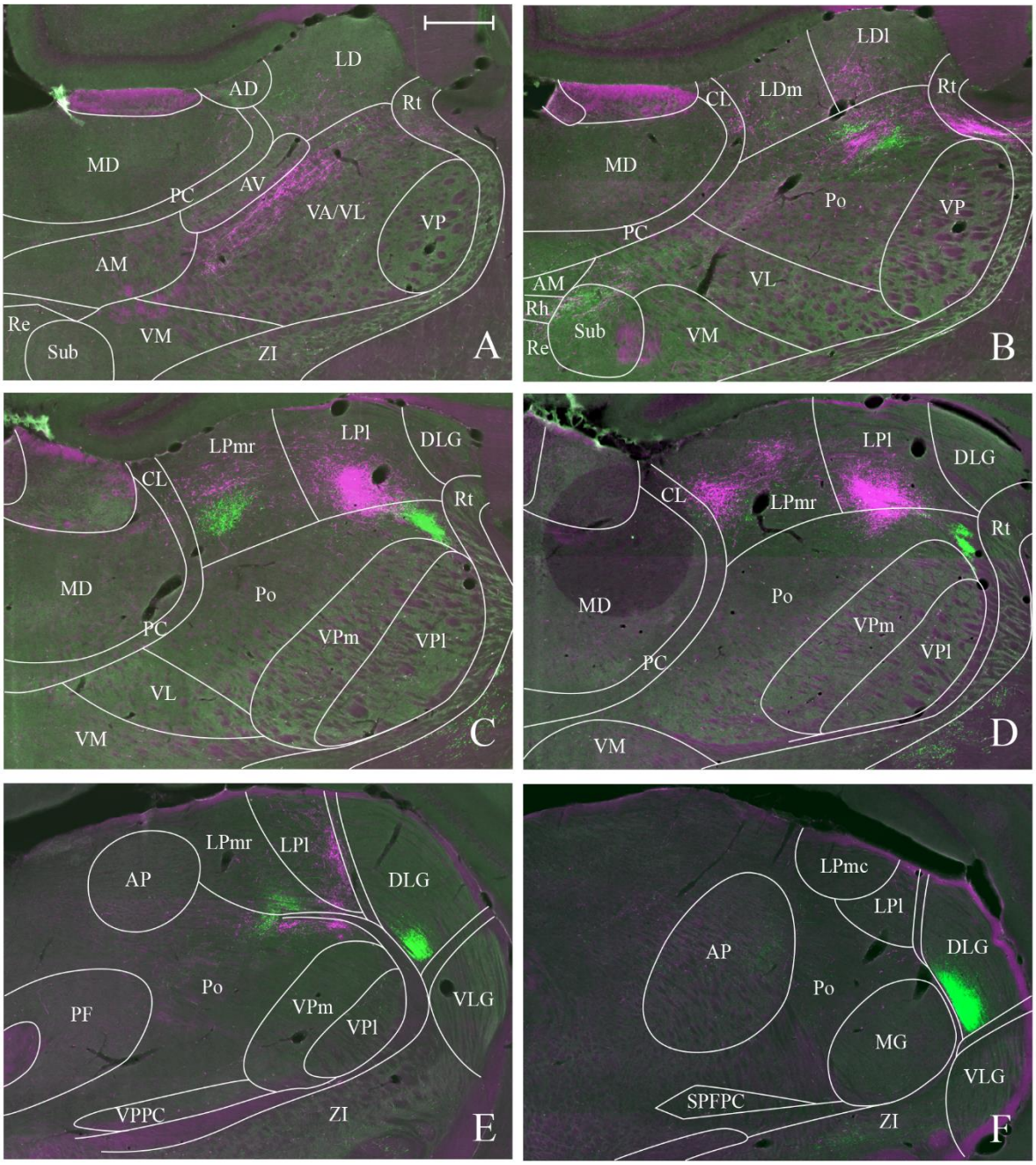


**Figure 20**. Anterogradely labeled fibers after injection of BDA (green fibers) in V1 and PHA-L (magenta fibers) in V2M. The BDA injection in V1 yielded a dense plexus of labeled fibers in DLG, while the PHA-L injection in V2M resulted in a high density of labeled fibers in LPmr and LPl. Scalebar 500 µm. See Table 2 for list of abbreviations.

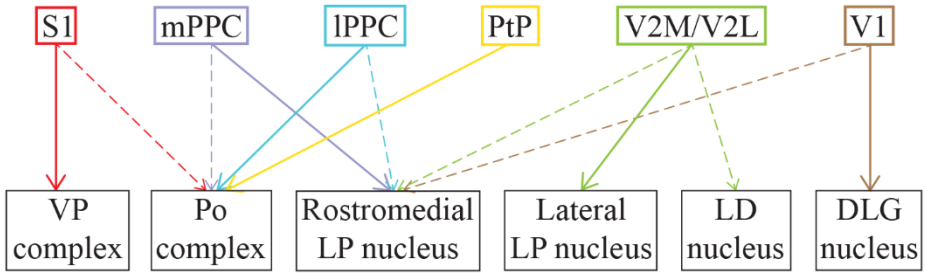


**Figure 21**. Summary of projections of areas in the dorsal caudal cortex to the thalamus in rat.

See Table 2 for list of abbreviations.